Gaia search for early-formed andesitic asteroidal crusts

M. Galinier, M. Delbo, C. Avdellidou, L. Galluccio, Y. Marrocchi

A&A 671, A40 (2023)
https://doi.org/10.1051/0004-6361/202245311

Astronomy & Astrophysics

Gaia search for early-formed andesitic asteroidal crusts

M. Galinier[1], M. Delbo[1], C. Avdellidou[1], L. Galluccio[1], and Y. Marrocchi[2]

[1] Université Côte d'Azur, CNRS–Lagrange, Observatoire de la Côte d'Azur, CS 34229, 06304 Nice Cedex 4, France
e-mail: marjorie.galinier@oca.eu
[2] CRPG, CNRS, Université de Lorraine, UMR 7358, Vandoeuvre-les-Nancy 54501, France

Received 28 October 2022 / Accepted 19 December 2022

ABSTRACT

Context. Andesitic meteorites are among the oldest achondrites known to date. They record volcanic events and crust formation episodes in primordial planetesimals that took place about 4.565 Myr ago. However, no analogue for these meteorites has been found in the asteroid population to date.
Aims. We searched for spectroscopic analogues of the andesitic meteorite Erg Chech 002 in the asteroid population using the *Gaia* DR3 spectral dataset.
Methods. In order to identify which asteroids have the most similar spectrum to Erg Chech 002, we first determined the spectral parameters of *Gaia* DR3 asteroids (spectral slope and Band I depth) and compared them to the spectral parameters of different samples of the meteorite. In addition, we performed a spectral curve matching between Erg Chech 002 and *Gaia* DR3 asteroid data, and we compared the results of both methods.
Results. We found that 51 main-belt asteroids have a visible spectrum similar to the one of Erg Chech 002, and 91 have a spectrum similar to the space-weathered spectra of the meteorite, corresponding to 0.08% and 0.15% of the whole *Gaia* DR3 dataset of asteroids with spectra, respectively. The asteroids that best match the laboratory samples of the meteorite are mostly located in the inner main belt, while the objects matching the space-weathered meteorite models show slightly more scattering across the belt.
Conclusions. Despite the fact that we find asteroids that potentially match Erg Chech 002, these asteroids are extremely rare. Moreover, a visible spectrum alone is not completely diagnostic of an Erg Chech 002-like composition. Near-infrared spectra will be important to confirm (or rule out) the spectral matches between Erg Chech 002 and the candidate asteroid population.

Key words. minor planets, asteroids: general – meteorites, meteors, meteoroids – techniques: spectroscopic

1. Introduction

Planetesimal accretion is considered the first stage of planetary formation. The composition and sizes of these planetesimals and the heliocentric distance of their accretion are key long-standing issues in planetary science (see, e.g. Johansen et al. 2015, and references therein). Planetesimal accretion took place during the first million years of our Solar System's history (Henke et al. 2012; Trieloff et al. 2022; Morbidelli et al. 2020, 2022), and the planetesimals that formed at the earliest times are expected to have been highly heated by the radioactive decay of ^{26}Al, and thus to be differentiated. During this process, the interior of a molten body with an initial homogeneous composition organises into layers of different densities and compositions, forming a dense metallic core, an olivine-rich overlaying mantle, and an igneous crust (e.g. McSween et al. 2002, and references therein). Subsequent collisional evolution fragmented those original planetesimals, producing families of asteroid fragments. These fragments should show different physical and spectral properties depending on the type of collision and the depth of the material excavation during the impact event. Moreover, family fragments can drift towards regions of orbital instability due to non-gravitational forces and then be delivered to Earth as meteorites.

Meteorites show a large range of compositions, reflecting the composition of the different layers of the parent body from which they are derived, if differentiated (e.g. Greenwood et al. 2020). Linking meteorites to asteroids provides insights into the internal structure of the parent body and into its accretion time and region. However, only a few links have been established up to now: the Howardite-Eucrite-Diogenite meteorites (HEDs) have been linked to the asteroid (4) Vesta and its family (Russell et al. 2012); the aubrite meteorites (enstatite achondrites) have been connected to the (434) Hungaria family (Lucas et al. 2019); and very recently the enstatite chondrite meteorites of EL type were linked to the asteroid family of (161) Athor (Avdellidou et al. 2022). All of these families are located in the inner main belt (i.e. with a semi-major axis between 2.1 and 2.5 au).

The study of HEDs, for example, showed that they originate from the igneous crust of asteroid (4) Vesta (e.g. McCord et al. 1970; Russell et al. 2012, 2013; Binzel et al. 1993; Burbine et al. 2001; de Sanctis et al. 2012), which is known to be differentiated (e.g. Ruzicka et al. 1997; Righter & Drake 1997; Mandler & Elkins-Tanton 2013). However, other eucrite meteorites that do not belong to the HEDs and thus do not come from Vesta have also been identified (Bland et al. 2009). Moreover, lithological, colour, and albedo differences have been detected by Mansour et al. (2020) between the vestoids, other low inclination basaltic asteroids of the inner belt, as well as basaltic asteroids with orbits beyond 2.5 au. All of these point to the necessary existence of another basaltic source of meteorites. Oszkiewicz et al. (2015) suggest that this object could be the parent body of the Flora family.

Despite the evidence given by the meteorites, few signs of differentiation amongst asteroids have been found to date. Searches for a population of basaltic crust-like asteroids (in and

outside the Vesta family; e.g. Moskovitz et al. 2008; Solontoi et al. 2012; Leith et al. 2017) as well as metallic ones (e.g. Harris & Drube 2014) have been successful. However, there is an observational lack of mantle-like olivine-rich asteroids in the main belt (DeMeo et al. 2019). These asteroids are identified as A types (Bus & Binzel 2002; DeMeo et al. 2009); in addition compared to the amount of basaltic and metallic asteroids in the main belt, they should be found in a larger proportion than what has been observed so far. This long-standing issue in planetary science is the so-called missing mantle problem (Chapman 1986).

Another interesting class of meteorites has been recently identified as evidence of differentiation in the main belt, in addition to the aubrites, iron meteorites, HEDs, and eucrites: the so-called andesitic meteorites (Day et al. 2009; Barrat et al. 2021). The formation mechanism of these meteorites is consistent with rapid cooling of a silicate-rich magma at the surface of a planetesimal. However, said mechanism is still debated (Arculus et al. 2009). In particular, the meteorite Erg Chech 002 (hereafter EC 002) found in May 2020 in the Sahara desert is reported by Barrat et al. (2021) to be 'the oldest andesite of the Solar System', with a measured crystallisation age of 4,565 Myr (around 2.25 Myr after the beginning of the Solar System). It has been classified as an ungrouped achondrite and it is spectroscopically unique. Its composition is similar to those experimentally produced by low partial melting of ordinary chondrite-like materials (Collinet & Grove 2020). This suggests that EC 002 could originate from the igneous crust of a non-carbonaceous planetesimal that suffered from low partial melting. This crust is thought to have been separated from the original parent body by a violent event, as suggested by evidence of a rapid cooling. EC 002 was thrown into space and travelled as part of a bigger body, before separating from it. As its composition is different from the HEDs, this meteorite provides evidence that some planetesimals were covered in andesitic and not basaltic crusts, the process of differentiation thus being different for these bodies.

The parent bodies of andesitic meteorites and planetesimals with andesitic crusts are unknown to date. Barrat et al. (2021) searched for objects with similar properties to EC 002 among the main belt asteroid population. To do so, they compared laboratory spectra of different samples of EC 002 to astronomical spectra of asteroids with strong pyroxene signatures, namely taxonomic end members of classes O and V, and to spectrophotometric data from the Sloan Digital Sky Survey (SDSS). No satisfying match between the meteorite and the asteroids was found. The authors concluded that almost the entire original population of planetesimals must have disappeared, as well as their fragments. They speculate that the disappearance of EC 002-like objects could be due either to their accretion to other asteroids to form larger planetary embryos, or to their destruction. This could also result from their erasure by subsequent stages of melting and planetary accretion and differentiation (Collinet & Grove 2020).

Reflectance spectra of EC 002 were acquired by Barrat et al. (2021). These spectra show the presence of two strong absorption bands that were linked to Ca-rich pyroxene: a first band centred around 0.95 µm (Band I), and a second one around 2 µm (Band II). They also show the presence of a small band centred around 0.65 µm, whose origin is not discussed by Barrat et al. (2021). However, the analysis done by the authors show that the pyroxenes of EC 002 are quite rich in Cr-bearing species (as shown in Table S2 of their supplementary material); and according to Moskovitz et al. (2008), Cloutis et al. (2018) and Cloutis (2002), Cr-rich high-Ca pyroxene can lead to the apparition of absorption features near 450 and 0.65 µm. Thus, the 0.65 µm absorption band observable in the reflectance spectrum of EC 002 could be due to the presence of chromium in the pyroxene of the meteorite. Comparing this spectrum with available asteroids spectra, the authors found no known asteroid spectral type presenting such absorption signatures.

In this work, we take advantage of the recent publication of an unprecedented sample of asteroid spectra by the Data Release 3 (DR3) of the ESA mission *Gaia* (Gaia Collaboration 2023) to search for analogues of EC 002 in the asteroid population. In Sect. 2, the dataset of asteroid spectra used is presented, along with the spectral data of the meteorite retrieved from Barrat et al. (2021). The methods are detailed in Sect. 3. In Sect. 4, we present our results, followed by a discussion in Sect. 5.

2. Data

In order to search for analogues of EC 002 among the asteroid population, we used the dataset of reflectance spectra that was acquired by *Gaia* between 5 August 2014 and 28 May 2017, and was released in June 2022. This dataset consists of mean reflectance spectra in the visible wavelength range of 60 518 Solar System objects (SSOs), with the majority of objects having magnitudes between ≃18 and 20. This is an unprecedented dataset of objects that are usually too faint to be observed from ground-based telescopes.

The reflectance spectra are acquired by two low-resolution slit-less spectrophotometers on board *Gaia*, the blue and red spectrophotometers (BP and RP), which are respectively optimised for the blue and red part of the spectrum. Specifically, the BP spans the wavelength range from 0.33 to 0.68 µm and the RP covers the range from 0.64 to 1.050 µm. The spectral resolution of each spectrophotometer is a function of wavelength, and varies from 4 to 32 nm pixel^{-1} for the BP and 7 to 15 nm pixel^{-1} for the RP (Gaia Collaboration 2023; Carrasco et al. 2021; Jordi et al. 2010). When an SSO transits on the focal plane of *Gaia* at a given epoch, each spectrophotometer measures counts at every wavelength to create 'epoch spectra'. Given that the wavelength range of both instruments overlaps in the 0.65–0.68 µm interval, the two epoch spectra are merged to create a full epoch spectrum. To each SSO is associated a unique mean reflectance spectrum obtained by averaging several epoch spectra, spanning the visible wavelength range from 374 to 1034 nm in 16 discrete wavelength bands (Gaia Collaboration 2023). A 'spectral_validation_flag' (hereafter flag) number is associated to each band, assessing the estimated quality of the band. In some cases, the merging of the epoch spectra taken by each spectrophotometer is not perfect and can lead to the creation of artefact bands (see Gaia Collaboration 2023). Caution must thus be taken when analysing the mean reflectance spectra in the overlapping wavelength interval. In a similar way, the bluest and reddest data bands of *Gaia* spectra are in general affected by large systematics due to the low efficiency of the spectrophotometers in these bands. They are not always flagged but they need to be taken with caution as well. To assess the quality of the asteroid analogues of EC 002 found using *Gaia* data, visible (VIS) and near-infrared (NIR) spectra from the literature were used in our analysis.

To perform our analysis, we used the EC 002 spectra that were published by Barrat et al. (2021). Barrat et al. (2021) acquired visible and near-infrared reflectance spectra of one powder sample and three raw slabs samples of EC 002. The spectra were digitised from the supplementary material of Barrat et al. (2021) using the region features (points and box) of the SAO Image DS9 software. A python code was used to transform

the pixel coordinates to reflectance and wavelengths units, and we verified that our digitised spectra were indistinguishable from the original ones before conducting the study. The spectra of the laboratory samples of the meteorite were later kindly provided to us by Jean-Alix Barrat and his co-authors (J. A. Barrat, P. Beck, priv. comm.). Since asteroid surfaces can be altered by space weathering and in order to compare the meteorite spectrum with asteroid spectra, Barrat et al. (2021) applied a space weathering model (Hapke 2001) to the powder sample of the meteorite, to simulate the effects of solar wind ion bombardment and micrometeorite impacts on the surface of the body. They published three space-weathered spectra of EC 002 corresponding to three different levels of space weathering – low, medium, and high – which we retrieved using SAO image DS9 software. In our study, we used the four reflectance spectra of the laboratory samples of the meteorite and the three modelled space-weathered spectra to search for asteroids with similar features to EC 002.

In order to compare our work with the one of Barrat et al. (2021), we also performed some comparison tests between the SDSS and the *Gaia* dataset. The SDSS dataset used in this work contains information for 33 584 asteroids and was retrieved from the work of DeMeo & Carry (2013). No selection criteria was applied to filter out noisy data, regardless of the uncertainties of the SDSS dataset.

3. Methods

In order to identify a spectral link between EC 002 and *Gaia* asteroids, we first compared the laboratory spectra of EC 002 to *Gaia* spectra without considering the effect of space weathering. Since the source of this meteorite is yet unknown, there is a probability that this object originates from a family of young fragments created by a recent collision. These fragments would have suffered limited space weathering because of their young age, showing a spectrum similar to the one of EC 002. Moreover, we present here an attempt to detect asteroids with similar spectral features as of EC 002 (similar spectral slope, presence of a pyroxene band around 0.95 µm and of a small 0.65 µm band), and these features are more easily detected without space weathering. It is also reasonable to believe that asteroids have surface grains. Given that they influence the spectroscopic properties of a medium, we studied the spectra of the powder and raw slab samples of EC 002.

On the other hand, EC 002 has the composition of a partial melt of an ordinary chondrite (Barrat et al. 2021). Once weathered, ordinary chondrites are spectrally similar to S-type asteroids. If the asteroids matching EC 002 suffered from space weathering, it is not unreasonable to expect a S-type-like space weathering (as expressed by the space weathering trend assumed by Barrat et al. 2021). Hence, we studied in a second time the modelled space-weathered spectra of EC 002. To summarise, we searched for asteroids spectrally matching the powder, raw slabs samples, and modelled space-weathered spectra of EC 002. To do so, we used two spectral matching methods described below.

3.1. Band I depth vs. slope comparison

The first method consists in comparing the spectral parameters derived from the reflectance spectra of the meteorite and of the asteroids. These parameters are the slope of the reflectance spectrum between 468.6 and 748 nm, and a measure of the depth of the silicate band centred around 950 nm (Band I depth). This method was inspired by the works of Barrat et al. (2021), DeMeo & Carry (2013) and Parker et al. (2008) using the SDSS asteroid spectrophotometric data. Ivezić et al. (2001) and Nesvorný et al. (2005) performed a principal component analysis on these data and identified two spectral parameters that express most of the data variability: the $a*$ parameter and the $i - z$ colour. The $a*$ parameter closely represents the slope of the reflectance spectrum in the g', r' and i' SDSS bands (Ivezić et al. 2001), these bands being respectively centred at 468.6 nm, 616.6 nm and 748.0 nm (DeMeo & Carry 2013). The $i - z$ colour is sensitive to the depth of a potential 1 µm band, the colour being the difference of magnitude between the i' and z' bands. These parameters are useful to characterise a visible asteroid spectrum.

DeMeo & Carry (2013) used slightly different spectral parameters to characterise the asteroids: the z-i parameter and the gri-slope. To evaluate them, the SDSS observed magnitudes of asteroids are converted into reflectance values at the centre of each SDSS filter, and the derived reflectance spectra are normalised to unity at the central wavelength of the g' filter (468.6 nm). The gri-slope is defined as the slope of the derived reflectance spectra over the g', r' and i' filters. The z-i parameter still measures the depth of a potential 1 µm band, but it is here defined as:

$$R_z - R_i = R(\lambda = 893.2\ \text{nm}) - R(\lambda = 748.0\ \text{nm}). \quad (1)$$

The gri-slope and $z - i$ colour of asteroids have been used to group objects into classes since (Ivezic et al. 2002; Carvano et al. 2010; DeMeo & Carry 2013). We note that the parameter measuring the Band I depth used in this study is a difference of reflectance, we therefore refer to it as $R_z - R_i$.

In order to compare *Gaia* reflectance spectra with what has been done in the work of Barrat et al. (2021), we evaluated the gri-slope and $R_z - R_i$ parameters for *Gaia* spectra. First, each *Gaia* spectrum was interpolated using a cubic smoothing spline (python3 package csaps, default smoothing parameter) and re-sampled between 450 and 900 nm. During this smoothing procedure, only *Gaia* bands with flags equal to zero (good quality bands) were considered and the first and last *Gaia* bands were not taken into account, in order to limit the impact of low quality bands on the calculated reflectance values. The re-sampled *Gaia* spectra were then normalised at 468.6 nm, and the spectral gri-slope was computed by linearly fitting the spectrum between 468.6 and 748.0 nm (first-degree polynomial fit, numpy package polyfit). The $R_z - R_i$ parameter was computed by taking the value of the reflectance of every re-sampled normalised *Gaia* spectra at the central wavelength of the i' and z' SDSS filters, namely 748.0 nm and 893.2 nm. The asteroids defined as potentially matching the spectrum of EC 002 are those in an area close to the meteorite in the $R_z - R_i$ vs. gri slope diagram. This will be further discussed in Sect. 4.

3.1.1. Asteroid matching with spectra of laboratory samples of EC 002

First, we studied the four laboratory samples of the meteorite EC 002 without taking space weathering into account. To compare the meteorite spectra with those of *Gaia* asteroids, their spectral slope and $R_z - R_i$ parameter were calculated. To do so, the spectrum of each sample was interpolated between 450 and 900 nm using a cubic smoothing spline (python3 package csaps, default smoothing parameter), as was done for the *Gaia* data. The spectra were then normalised to unity at 468.6 nm and the $R_z - R_i$ parameter was calculated using Eq. (1). The spectral slope was evaluated between 468.6 and 748.0 nm applying

Table 1. Spectral slope and Band I depth evaluated for different samples of EC 002.

Sample	Spectral slope (%(100 nm)$^{-1}$)	$R_z - R_i$
Powder	24.3	–0.74
Raw slab 1	27.4	–0.77
Raw slab 2	20.1	–0.75
Raw slab 3	27.1	–0.80

a first degree polynomial fit. The value of these two parameters for the powder and raw slabs samples of EC 002 are available on Table 1.

In order to identify the asteroids with spectral parameters similar to EC 002, we calculated the average of the slope and $R_z - R_i$ values for the four samples. The corresponding point is considered as the 'barycentre' of the non-space-weathered samples. Then, we determined a 3σ confidence ellipse around this barycentre. The equation of the confidence ellipse centred on a barycentre of coordinates (x_c, y_c) and oriented with an angle α is:

$$\left(\frac{\cos^2\alpha}{a^2}+\frac{\sin^2\alpha}{b^2}\right)(x-x_c)^2+\left(\frac{\sin^2\alpha}{a^2}+\frac{\cos^2\alpha}{b^2}\right)(y-y_c)^2$$
$$+2(x-x_c)(y-y_c)\sin\alpha\cos\alpha\left(\frac{1}{b^2}-\frac{1}{a^2}\right)=s, \quad (2)$$

with x the gri-slope of a reflectance spectrum, $y = R_z - R_i$, and s the scale of the ellipse that represents a chosen confidence level. a and b are respectively the semi-major and semi-minor axis of the ellipse. It is possible using χ-square probabilities to determine that for a 3σ ellipse, the s value is 9.210 (99% confidence level). If an asteroid falls inside the 3σ ellipse in the spectral parameter space, then it would be considered as a candidate match of EC 002 according to its visible spectrum.

To compute the parameters of the 3σ confidence ellipse, we calculated the covariance matrix of the four laboratory samples of the meteorite. The semi-major and semi-minor axis of the ellipse are defined as:

$$\begin{cases} a &= \sqrt{s\lambda_1} \\ b &= \sqrt{s\lambda_2}, \end{cases} \quad (3)$$

with λ_1 and λ_2 the eigenvalues of the covariance matrix, λ_1 being the largest. The angle α of the ellipse is defined as $\alpha = \arctan\frac{v_1(y)}{v_1(x)}$ with v_1 the eigenvector of the covariance matrix associated to the largest eigenvalue.

3.1.2. Asteroid matching with modelled space-weathered spectra of EC 002

After studying non-space-weathered samples of EC 002, we analysed the modelled spectra of EC 002 from Barrat et al. (2021) on which was applied the Hapke (2001) space weathering model (from Fig. S12 of the supplementary material of Barrat et al. 2021). The slope and $R_z - R_i$ parameters were calculated for these spectra, following the same procedure as explained before. In order to study more stages of space weathering of the meteorite, we fitted a straight line to the points corresponding to the powder sample and to the three space-weathered samples in the $R_z - R_i$ vs. slope plot. This line will be referred in the following as the 'space weathering line'. A parallel line to the space weathering line centred on the barycentre of the non-weathered samples was calculated, and the 3σ ellipse was moved along this line from the lowest to the highest space weathering points, in order to define a 'possible matches area' within which objects could present spectral parameters similar to those of EC 002 with different levels of space weathering. The spectra of the asteroids within this 'possible matches area' were then visually inspected. Indeed, we preferred relying on visual inspection rather than on an automated method to assess the quality of the matches, firstly because of the relatively small number of objects to inspect and secondly because the 0.65 µm band present on the meteorite spectrum was never detected by algorithms. This band being a characteristic feature of the meteorite spectrum, we chose the method where its presence was the most surely detected.

3.2. Curve matching

The second method we used in order to find spectral analogues of EC 002 is a curve matching method, between the meteorite and the asteroids reflectance spectra. This method is widely used in the literature (see, e.g. Popescu et al. 2012; DeMeo et al. 2022). It consists in evaluating how similar two spectra are relying on the measure of a best-fit coefficient. In this work, among the possible existing coefficients, we chose to use the χ^2 goodness-of-fit test. The reduced χ^2 we used is expressed as:

$$\chi^2_{\rm red} = \frac{1}{\nu}\sum_i^N \frac{(A_i - f.M_i)^2}{\sigma_i^2}, \quad (4)$$

with M_i the meteorite spectrum, A_i a *Gaia* asteroid reflectance spectrum and σ_i its associated uncertainties, ν the number of degrees of freedom, and f a normalisation factor allowing the best overlap between the meteorite and *Gaia* reflectance spectra. The f-value was determined by minimising the $\chi^2_{\rm red}$ such that the partial derivative of the $\chi^2_{\rm red}$ with respect to f is zero. This leads to:

$$f = \frac{\sum_i^N \frac{M_i.A_i}{\sigma_i^2}}{\sum_i^N \frac{M_i^2}{\sigma_i^2}}. \quad (5)$$

In order to compare EC 002 with asteroids, we started by sampling the meteorite spectrum at *Gaia*'s wavelengths. We considered only the good quality bands in *Gaia* spectra. Since the bands at the extreme wavelengths of the spectral range are often damaged due to the low BP-RP sensitivity there, the first and last bands of *Gaia* spectra were not taken into account. Moreover, as explained earlier, DR3 SSO spectra were assigned a non-zero flag to the bands where some potential problems were detected. Every band flagged with a non-zero number was removed. The 'cleaned' *Gaia* spectra were thus composed of 14 bands spanning the wavelength range from 418 to 990 nm, provided that they had a flag = 0.

Then, a cubic smoothing spline was applied to the meteorite spectrum to interpolate it (python package csaps, smoothing parameter of 0.0001) and the interpolated spectrum was sampled as each cleaned *Gaia* spectrum. This re-sampled meteorite spectrum was then normalised at 550 nm. Figure 1 shows the different spectra of EC 002 normalised and re-sampled.

For each sample of the meteorite, the χ^2_{red} of Eq. (4) was calculated between each cleaned asteroid spectrum and the re-sampled and re-normalised meteorite spectrum. As explained in previous studies (Hanuš et al. 2015, 2018), a 3σ match to the

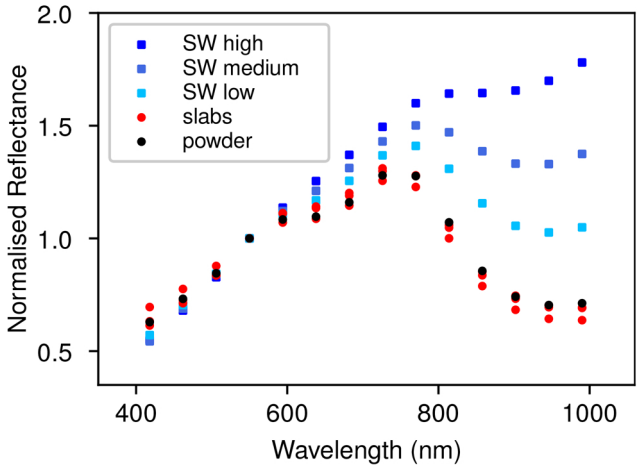

Fig. 1. Spectra of a powder, three raw slab samples and three modelled spectra of space-weathered of EC 002 sampled and normalised as *Gaia* data, after removing the first and last *Gaia* bands.

Table 2. Accepted asteroids as candidate matches for the different samples of EC 002, according to the method used.

Sample	Spectral parameter	CM	Total
Powder + slabs	41	18/10	51
SW low	56	23/15	71
SW medium	12	8/5	17
SW high	2	1/1	3

Notes. CM stands for curve matching. The first number in the CM column is the number of asteroids found using the curve matching method for a given sample of the meteorite, and the second number corresponds to the number of asteroids not already found with the spectral parameter method. The total number of matches for each sample is indicated in the last column.

meteorite is defined as an asteroid respecting the following condition: $\chi^2_{\rm red} < 1 + 3\sigma$ with $\sigma = \frac{\sqrt{2\nu}}{\nu}$ and ν the number of degrees of freedom. For ν=16, $\chi^2_{\rm red} < 2.06 \simeq \chi^2_{\rm red} < 2$. For each meteorite sample, the best matches were selected according to this criterion and their spectra were then visually inspected.

4. Results

In this section, we describe the results from (i) the comparison of the spectral slope and Band I depth, and (ii) the curve matching method, between the spectra of EC 002 and that of *Gaia* asteroids. As it will be shown, some asteroids were identified as having *Gaia* reflectance spectra similar to the visible part of the spectrum of EC 002. The number of matches found with each method and each sample is recapitulated on Table 2, and the detail of the number and name of each asteroid matching and with which method it was found is given on Table 3.

4.1. SDSS-Gaia spectral parameters comparison

First, because Barrat et al. (2021) did not find satisfactory matches between EC 002 and the SDSS data, we started our analysis by investigating potential differences between *Gaia* and the SDSS dataset. To compare them, we calculated the spectral slope and the $R_z - R_i$ parameter for every object in each dataset. The spectral slope was computed by linearly fitting the three SDSS reflectance data points in the g, r and i SDSS filters using a one-degree polynomial fit (numpy polynomial.polyfit). The same spectral parameters were calculated for the 60 518 *Gaia* spectra as explained in Sect. 3.

As can be seen in Fig. 2, the two datasets appear to be shifted in the spectral parameter space. In order to study these apparent shifts, we used a sub-sample of 14 129 asteroids having observations both in *Gaia* and SDSS. Figure 3 shows histograms of the spectral parameters of this sub-sample, where a shift in $R_z - R_i$ is clearly visible on panel (B). To evaluate the value of this shift, the median value of $R_z - R_i$ was calculated for both datasets of the sub-sample and we found that *Gaia* data have 0.076 times higher $R_z - R_i$ than the SDSS, doing the difference of the two. While there is a general agreement in spectral slope between the two surveys (difference between median slope of both surveys of only 0.52), a wing of higher slope values for *Gaia* asteroids can be noticed in Fig. 3 (A), meaning that *Gaia* detects objects redder than the SDSS. The shift in $R_z - R_i$ is quite significant and remains when considering only objects with a high S/N ($S/N > 100$ for example). We chose not to correct *Gaia* data from this shift in this work since we do not know its causes.

A potential reason for this shift could be the different choice of solar analogues between the two surveys. Indeed, a mean solar analogue spectrum was used to retrieve the asteroids spectra from *Gaia*, and solar colours are needed to convert colour indices to reflectances for the SDSS. It is possible that the accuracy of the solar analogues or the solar colours used is at the origin of this shift. This difference between the SDSS and *Gaia* will be investigated in future works.

4.2. Spectral parameter matching

In the following are described the potential matches of EC 002 obtained with the study of spectral parameters. The slope and $R_z - R_i$ spectral parameters were calculated for the spectra of the powder sample and all raw slab samples of EC 002 (see Table 1). The average and standard deviation for the slope and Band I depth are of 24.7 ± 2.9% (100 nm)$^{-1}$ and −0.76 ± 0.02, respectively. In Fig. 4, the corresponding point is plotted as an orange diamond. We can observe that the points corresponding to the different samples of the meteorite plots away from any group of asteroids in the spectral parameter space, as already observed in Fig. S14 of the supplementary material of Barrat et al. (2021).

In the spectral parameter space, using the average point as a centre, we defined a 3σ confidence ellipse as described in Sect. 3 in which no asteroid is contained (Fig. 4). As described in Sect. 3, we calculated a 'space weathering line' of equation: $y = 0.047x - 1.92$. The coefficient of determination of this fit is $R^2 = 0.986$, meaning that the linear fit to the space weathering modelled spectra of Barrat et al. (2021) is good. This line plots to the right side of the spectral parameter space, where only a few asteroids are present.

Using the parameters of the linear fit, we extended the 3σ ellipse along the space weathering line, defining a 'possible matches area' that contains 305 asteroids listed in Table A.1, which spectra were visually inspected.

Following several criteria we rejected ~63.8% of the sample. As a first step, we rejected the objects that have known VIS or NIR spectrum in the literature that allowed to distinguish them from EC 002. It corresponds to 10.2% of the initial sample of 305 asteroids. Then, we removed the objects with more than three flagged bands in the *Gaia* spectrum (1.8% of the sample). Finally, we rejected the asteroids that had either a too noisy spectrum, or that were visually different from the spectra of EC 002

Table 3. Accepted asteroids as candidate matches for the different samples of EC 002.

Asteroid	Method
Powder + raw slabs	
(1643) Brown	Spectral parameters
(1946) Walraven	Spectral parameters
(2432) Soomana	Spectral parameters
(3188) Jekabsons	Spectral parameters
(3651) Friedman	Spectral parameters
(3869) Norton	Spectral parameters
(4302) Markeev	Spectral parameters
(5121) Numazawa	Spectral parameters
(6853) Silvanomassaglia	Spectral parameters + CM
(6876) Beppeforti	Spectral parameters
(8587) Ruficollis	Spectral parameters
(8827) Kollwitz	Spectral parameters
(9197) Endo	Spectral parameters
(9433) 1997 CF3	Spectral parameters
(10156) 1994 VQ7	Spectral parameters + CM
(10671) Mazurova	Spectral parameters
(10902) 1997 WB22	Spectral parameters
(11155) Kinpu	Spectral parameters
(12551) 1998 QQ39	Spectral parameters
(13839) 1999 XF29	Spectral parameters
(15989) 1998 XK39	Spectral parameters
(16856) Banach	CM
(17056) Boschetti	CM
(17240) Gletorrence	Spectral parameters
(20454) Pedrajo	Spectral parameters + CM
(24286) 1999 XU188	Spectral parameters
(24892) 1997 AD3	Spectral parameters + CM
(26573) 2000 EG87	Spectral parameters
(27262) 1999 XT184	Spectral parameters
(28162) 1998 VD14	Spectral parameters
(30769) 1984 ST2	Spectral parameters
(33418) Jacksonweaver	Spectral parameters
(36431) 2000 PJ12	Spectral parameters
(44150) 1998 HC108	Spectral parameters
(47232) 1999 VQ36	Spectral parameters
(49101) 1998 RE76	Spectral parameters
(54062) 2000 GX135	CM
(55549) 2001 XC59	Spectral parameters + CM
(56904) 2000 QP171	Spectral parameters
(63653) 2001 QQ109	CM
(77147) 2001 EV6	CM
(77935) 2002 GM54	CM
(87093) 2000 LW6	Spectral parameters
(88955) 2001 TW42	Spectral parameters + CM
(89556) 2001 XS98	CM
(90604) 4813 P-L	Spectral parameters
(123113) 2000 SH361	CM
(124884) 2001 TE41	CM
(164121) 2003 YT1	CM
(205560) 2001 SC282	Spectral parameters + CM
(310436) 2000 AB169	Spectral parameters + CM
SW low	
(4088) Baggesen	Spectral parameters
(6003) 1988 VO1	Spectral parameters
(6789) Milkey	Spectral parameters
(8243) Devonburr	Spectral parameters
(8483) Kinwalaniihsia	Spectral parameters

Asteroid	Method
SW low	
(8692) 1992 WH	Spectral parameters
(9753) 1990 QL3	Spectral parameters
(10131) Stanga	CM
(11920) 1992 UY2	Spectral parameters
(14511) Nickel	Spectral parameters
(15088) Licitra	Spectral parameters
(15623) 2000 HU30	CM
(17739) 1998 BY15	Spectral parameters
(17821) Bolsche	Spectral parameters
(17882) Thielemann	Spectral parameters
(17943) 1999 JZ6	Spectral parameters
(18344) 1989 TN11	Spectral parameters
(18780) Kuncham	CM
(19978) 1989 TN6	Spectral parameters
(20289) Nettimi	Spectral parameters
(20535) Marshburrows	CM
(21318) 1996 XU26	Spectral parameters
(22276) Belkin	CM
(22538) Lucasmoller	CM
(23766) 1998 MZ23	Spectral parameters
(24569) 9609 P-L	Spectral parameters
(24684) 1990 EU4	Spectral parameters + CM
(26084) 1981 EK17	Spectral parameters
(26851) Sarapul	Spectral parameters
(27876) 1996 BM4	Spectral parameters + CM
(27884) 1996 EZ1	Spectral parameters
(28132) Karenzobel	Spectral parameters
(29171) 1990 QK3	Spectral parameters
(30426) Philtalbot	Spectral parameters
(30834) 1990 VR6	Spectral parameters
(32835) 1992 EO5	CM
(33423) 1999 DK	CM
(33852) Baschnagel	CM
(33934) 2000 LA30	CM
(33947) 2000 ML1	Spectral parameters + CM
(35364) Donaldpray	Spectral parameters
(39940) 1998 FR99	Spectral parameters
(41894) 2000 WH121	Spectral parameters
(43278) 2000 ES109	Spectral parameters + CM
(44162) 1998 HC148	Spectral parameters
(45787) 2000 OJ24	Spectral parameters
(48039) 2001 DT69	Spectral parameters
(51659) Robohachi	Spectral parameters
(53417) 1999 NP38	Spectral parameters
(53661) 2000 DU62	Spectral parameters
(53899) 2000 FM49	Spectral parameters
(56561) Jaimenomen	Spectral parameters + CM
(58640) 1997 WH18	Spectral parameters
(61098) 2000 LY28	Spectral parameters
(64458) 2001 VF35	Spectral parameters
(65504) 3544 P-L	CM
(74107) 1998 QM37	Spectral parameters
(74378) 1998 XH11	CM
(75323) 1999 XY47	Spectral parameters
(79827) 1998 WU3	CM
(87216) 2000 OG38	Spectral parameters
(89776) 2002 AL90	Spectral parameters

Table 3. continued.

Asteroid	Method
SW low	
(89952) 2002 JB20	Spectral parameters + CM
(92593) 2000 PN16	Spectral parameters
(100440) 1996 PJ6	CM
(103308) 2000 AH55	CM
(108139) 2001 GL11	Spectral parameters + CM
(112326) 2002 MM4	Spectral parameters + CM
(122122) 2000 JM16	Spectral parameters
(128450) 2004 NX24	Spectral parameters
(134916) 2000 YP53	Spectral parameters
SW medium	
(13133) Jandecleir	Spectral parameters
(18143) 2000 OK48	Spectral parameters
(31060) 1996 TB6	Spectral parameters
(42822) 1999 NT13	Spectral parameters + CM
(44322) 1998 RZ42	Spectral parameters + CM
(49141) 1998 SM41	Spectral parameters
(51379) 2001 BY7	Spectral parameters
(52408) 1993 TJ34	Spectral parameters
(68089) 2000 YS108	CM
(68946) 2002 PX138	CM
(90843) 1995 YZ22	Spectral parameters
(93797) 2000 WO43	CM
(99714) 2002 JQ41	Spectral parameters
(108899) 2001 PP5	CM
(122125) 2000 JO17	Spectral parameters
(145532) 2006 FD42	CM
(230762) 2003 WP192	Spectral parameters + CM
SW high	
(9974) Brody	Spectral parameters
(19754) Paclements	Spectral parameters
(33809) 1999 XK152	CM

Notes. Asteroids showing a spectrum matching the powder and raw slabs samples of the meteorite are 51 in number, while 71 asteroids match the low space-weathered spectrum of EC 002, 17 asteroids match its medium space-weathered spectrum and three asteroids match its highly space-weathered spectrum. CM stands for curve matching.

in either BP or RP parts (51.8% of the sample). For the last case we noticed that several spectra, otherwise similar to the one of EC 002 show a steep increase of the reflectance in the red part, making their Band I centre shifted compared to the one of the meteorite. We chose to reject such objects of the list of candidate matches.

After our visual inspection, 110 asteroids were retained (Table A.1). Among these validated asteroids, 106 objects have been given a spectrum for the first time by the *Gaia* mission, and 41 asteroids were identified to have a reflectance spectrum similar to the laboratory spectra of EC 002. These objects are defined as matches. The matches of the four laboratory samples of the meteorite were not considered separately here, because these samples show almost indistinguishable spectra in the visible wavelength range. The spectra of the matches are shown on Fig. B.1, and their median signal-to-noise ratio (S/N) is of 26.3.

In addition, there are 70 asteroids matching the space-weathered spectra of EC 002: 56 asteroids match the spectrum on which has been applied a low space weathering, 12 asteroids match the medium space-weathered spectrum and only two asteroids match the highly space-weathered spectra. Their spectra are shown respectively on Figs. B.2–B.4. The median S/N of the matches is of 23.0 for the low space-weathering of EC 002, of 18.2 for the median space weathering, and of 15.97 for asteroid (9974) Brody and 14.05 for asteroid (19754) Paclements.

4.3. Curve matching

We applied the curve matching method to the different laboratory spectra of the EC 002 (powder and slabs) and to the entire dataset of 60 518 *Gaia* asteroid reflectance spectra. As mentioned before, the matches of the four laboratory samples were not considered separately here due to the similar visible spectra of these samples.

We considered only the cases giving $\chi^2_{\rm red} < 2$, resulting in a list of 58 bodies matching EC 002 listed on Table A.2. After a visual inspection of their spectra, several objects were rejected (Table A.2). The final list of potential matches to EC 002 meteorite contains 18 asteroids. Amongst these, ten asteroids were not found with the spectral parameters method: (16856) Banach, (17056) Boschetti, (54062) 2000GX135, (63653) 2001QQ109, (77147) 2001EV6, (77935) 2002GM54, (89556) 2001XS98, (123113) 2000SH361, (124884) 2001TE41, and (164121) 2003YT1. The spectra of these ten bodies are shown on Fig. B.5.

The curve matching method was then applied to the space-weathered samples of EC 002. For the low space-weathered spectrum, 269 asteroids had a $\chi^2_{\rm red} < 2$. There was 223 asteroids with $\chi^2_{\rm red} < 2$ for the medium space-weathered spectrum, and only 12 asteroids for the highly space-weathered spectrum.

Most asteroids were rejected following the criteria exposed earlier. We finally found 23 asteroids as potential analogues of the low space-weathered EC 002, eight asteroids matching the medium space-weathered EC 002 and one asteroid matching the highly space-weathered meteorite. These objects are listed in Table A.3. The asteroids that were found as matches with this method and not with the spectral parameters method are asteroids (10131) Stanga, (15623) 2000 HU30, (18780) Kuncham, (20535) Marshburrows, (22276) Belkin, (22538) Lucasmoller, (32835) 1992EO5, (33423) 1999DK, (33852) Baschnagel, (33934) 2000LA30, (65504) 3544P-L, (74378) 1998XH11, (79827) 1998WU3, (100440) 1996PJ6, and (103308) 2000AH55 for the low SW; asteroids (68089) 2000YS108, (68946) 2002PX138, (93797) 2000WO43, (108899) 2001PP5, (145532) 2006FD42 and (230762) 2003WP192 for the medium SW and asteroid (33809) 1999XK152 for the high SW. Their spectra are shown respectively on Figs. B.6–B.8.

5. Discussion

Asteroids spectroscopically matching EC 002 are extremely rare. We find only 51 asteroids matching the non-space-weathered spectrum of EC 002, and 91 asteroids matching its spectrum on which was modelled the effect of space weathering to various degrees. Considering the entire *Gaia* sample of over 60 518 Solar System minor bodies, it means a mere 0.08% of the sample for the non-space-weathered samples and 0.15% of the sample for the space-weathered EC 002. This confirms the conclusions of Barrat et al. (2021) about the scarcity of analogues of EC 002 among the asteroid population.

The best matches of the different samples of EC 002 are defined as the objects found using both methods. For the four

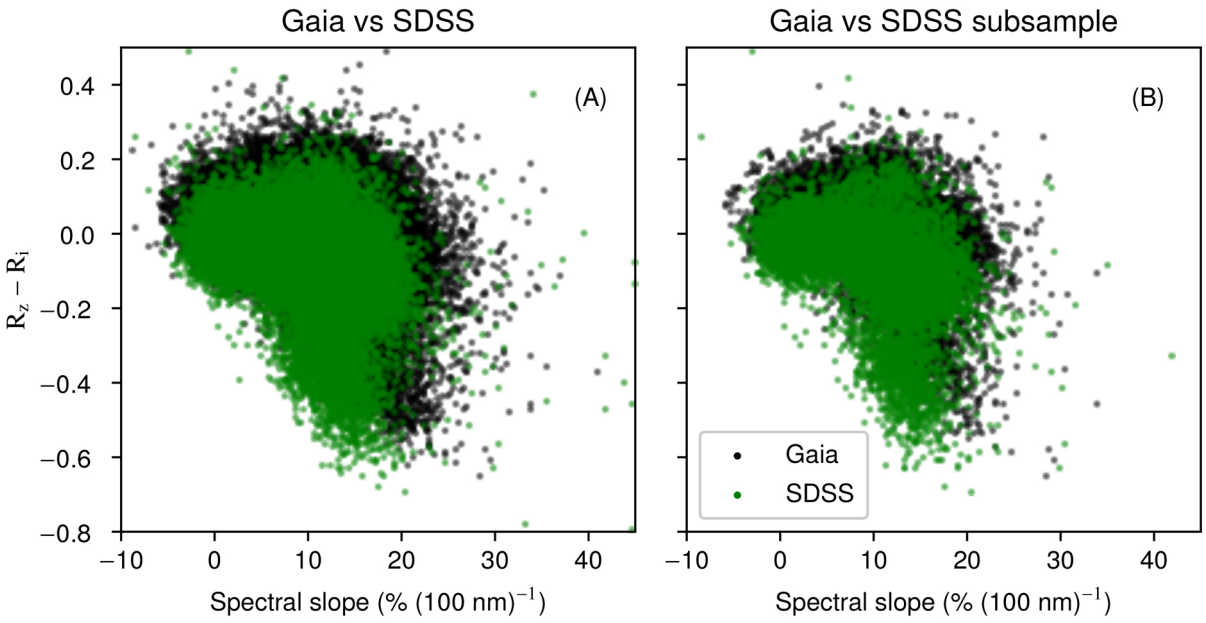

Fig. 2. Comparison of the Band I depth $R_z - R_i$ and the spectral slope for *Gaia* (black) and the SDSS (green) asteroids. Panel A: comparison between the 60 518 asteroids of *Gaia* and the 33 584 asteroids of the SDSS. Panel B: comparison between a sub-sample of 14 129 asteroids both observed by the SDSS and *Gaia*. A shift in $R_z - R_i$ between the spectra of *Gaia* and the SDSS is visible in both panels.

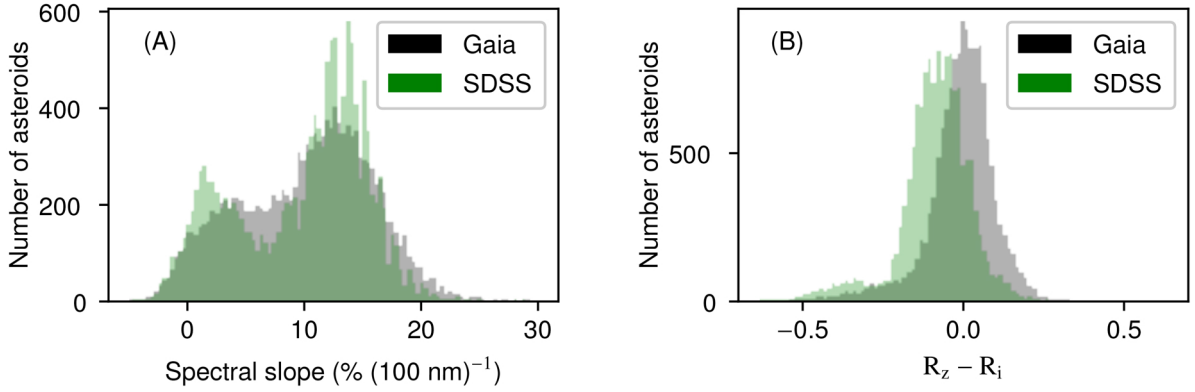

Fig. 3. Comparison of the $R_z - R_i$ parameter and of the spectral slope for the sub-sample of 14 129 asteroids observed both by *Gaia* and SDSS. We note that the slope distribution (panel A) of *Gaia* has a wing that extends to redder slopes than the SDSS. Panel B shows that the distributions of $R_z - R_i$ for *Gaia* and SDSS are clearly shifted, with *Gaia* seeing a less deep Band I compared to the SDSS. *Gaia* and SDSS $R_z - R_i$ parameter histograms can be superimposed when a constant value of 0.07 is subtracted from *Gaia* $R_z - R_i$-values.

laboratory samples, there are seven best matches: (6853) Silvanomassaglia, (10156) 1994VQ7, (20454) Pedrajo, (55549) 2001XC59, (88955) 2001TW42, (205560) 2001SC282, and (310436) 2000AB169. For the spectra on which was applied a low space weathering model, there are eight best matches: asteroids (24684) 1990 EU4, (27876) 1996BM4, (33947) 2000ML1, (43278) 2000ES109, (56561) Jaimenomen, (89952) 2002JB20, (108139) 2001GL11, and (112326) 2002MM4. For the medium space weathering model, asteroids (42822) 1999NT13, (44322) 1998RZ42, and (230762) 2003WP192 are found by both methods. No asteroid is found by both methods for the highly space-weathered spectrum.

Both methods give quite different asteroid as matches. Indeed, we did not filter the objects considering their S/N but we noticed that the large majority of objects retained as potential analogues of EC 002 have S/N-values lower than a hundred. For the curve matching method, the median value of the S/N for the accepted objects is of 17.2. This low value is explained by the fact that the chosen curve matching parameter favours observations with large error bars, hence low S/N observations. This method thus filters out objects with higher S/N found by the spectral parameter method that appear to be very good matches by visual inspection, such as asteroid (5121) Numazawa. In order to evaluate the results of this curve matching method, we performed some tests with an alternative Least Squares method. We computed the sum of the squared residuals between the meteorite and the asteroids spectra, removing the flagged points as was done for the $\chi^2_{\rm red}$ calculation and not taking the uncertainties into account. The sum of the squared residuals used is described in Eq. (6):

$$\mathrm{R}^2 = \sum_{\mathrm{i}}^{\mathrm{N}} (\mathrm{A_i} - \mathrm{f.M_i})^2, \tag{6}$$

with M_i the meteorite spectrum, A_i a *Gaia* asteroid reflectance spectrum and f a normalisation factor similar to the one in Eq. (5) but without consideration of the uncertainties. This

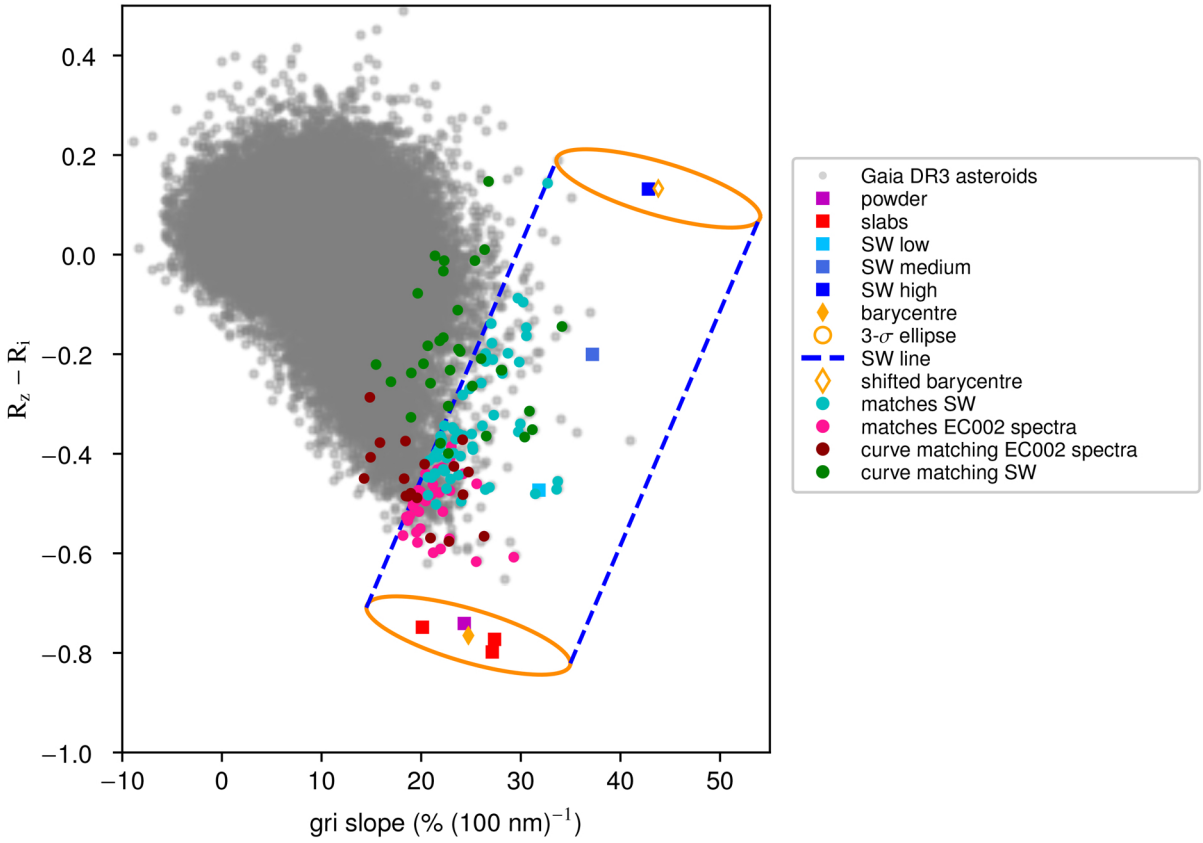

Fig. 4. Distribution of depth of the 1 µm band with respect to the spectral slope of every *Gaia* asteroid (grey dots). Red squares: raw slabs of the meteorite EC 002. Purple square: powder sample of the meteorite. Full orange diamond: barycentre of these four samples, and empty orange diamond: shifted barycentre along the 'space weathering line'. The squares going from light blue to dark blue represent the modelled space-weathered spectra of EC 002, with different space weathering intensity. The orange ellipses are the 3-σ ellipse respectively around the barycentre and shifted following the space weathering behaviour of EC 002. The two dashed blue lines delimit a 'possible matches area', within which are represented asteroids matching EC 002. Pink dots: asteroids matching the raw slabs and powder sample of EC 002. Cyan dots: asteroids matching the space-weathered samples. Dark red dots: asteroids matching EC 002 by the curve matching method. Green dots: asteroids matching the space-weathered spectra of EC 002 by this same method.

method spans a wider range of S/N, giving only potential matches of EC 002 among asteroids with S/N above 25 for the powder sample of the meteorite for example. Most asteroids found as potential matches plot inside the 'possible matches area' of Fig. 4 and thus were already found with the spectral parameters method. This method is therefore a complement of the spectral parameter method, but since it is sensitive to outliers it requires a visual inspection as well to assess the quality of the matches. The curve matching method with the $\chi^2_{\rm red}$ has the advantage that it explores a larger area in the spectral parameter space, finding objects outside the 'possible matches area' even though they are low S/N asteroids. These objects should be further observed and studied in future analysis to evaluate how good a match they are.

All matched asteroids with the non-space-weathered meteorite spectra are located in the inner part of the main belt (Fig. 5), between the secular resonance ν_6 and the 3:1 mean motion resonance with Jupiter. The asteroids matched with the space-weathered meteorite are more scattered across the main belt, even though most objects can be found in the inner main belt as well, in particular close to the Vesta family (Fig. 6).

Some of the asteroids matching the different samples of EC 002 are members of known collisional families, according to the membership of Nesvorný et al. (2015). Among the 142 matches of the different samples of EC 002, 23.9% of the asteroids belong to the Vesta family, 9.8% belong to the Flora family and a mere 7.7% belong to other families (mainly Nysa-Polana).

The presence of asteroids matching with EC 002 inside the Vesta family could be due to two possible reasons. If these objects are real analogues to EC 002, they could be interlopers inside the Vesta family since EC 002 is chemically distinct from the HEDs (Barrat et al. 2021). The second possibility is that these asteroids are true Vesta family members compositionally alike HEDs, but which happen to have a *Gaia* reflectance spectrum in the visible range very similar to that of EC 002. In fact, the distinction between the reflectance spectra of EC 002 and HEDs in the visible is difficult, and relies mainly on the position of the Band I centre. However, the last *Gaia* bands may show a fast increase in reflectance due to light contamination in the RP (Gaia Collaboration 2023). This contamination could result in a shift of the Band I centre. Future analysis of the *Gaia* reflectance spectra could help solve this issue, and future near-infrared spectroscopy of these bodies might be able to reveal if they are more similar to EC 002 or to the HEDs and to Vesta family members.

The Flora family is a large collisional family adjacent to the ν_6 (Nesvorný et al. 2015), which is the most efficient region to deliver main-belt asteroids to Earth-crossing orbits (Granvik et al. 2016). Hence, this family could be an important source of near-Earth asteroids (La Spina et al. 2004; Kryszczyńska 2013)

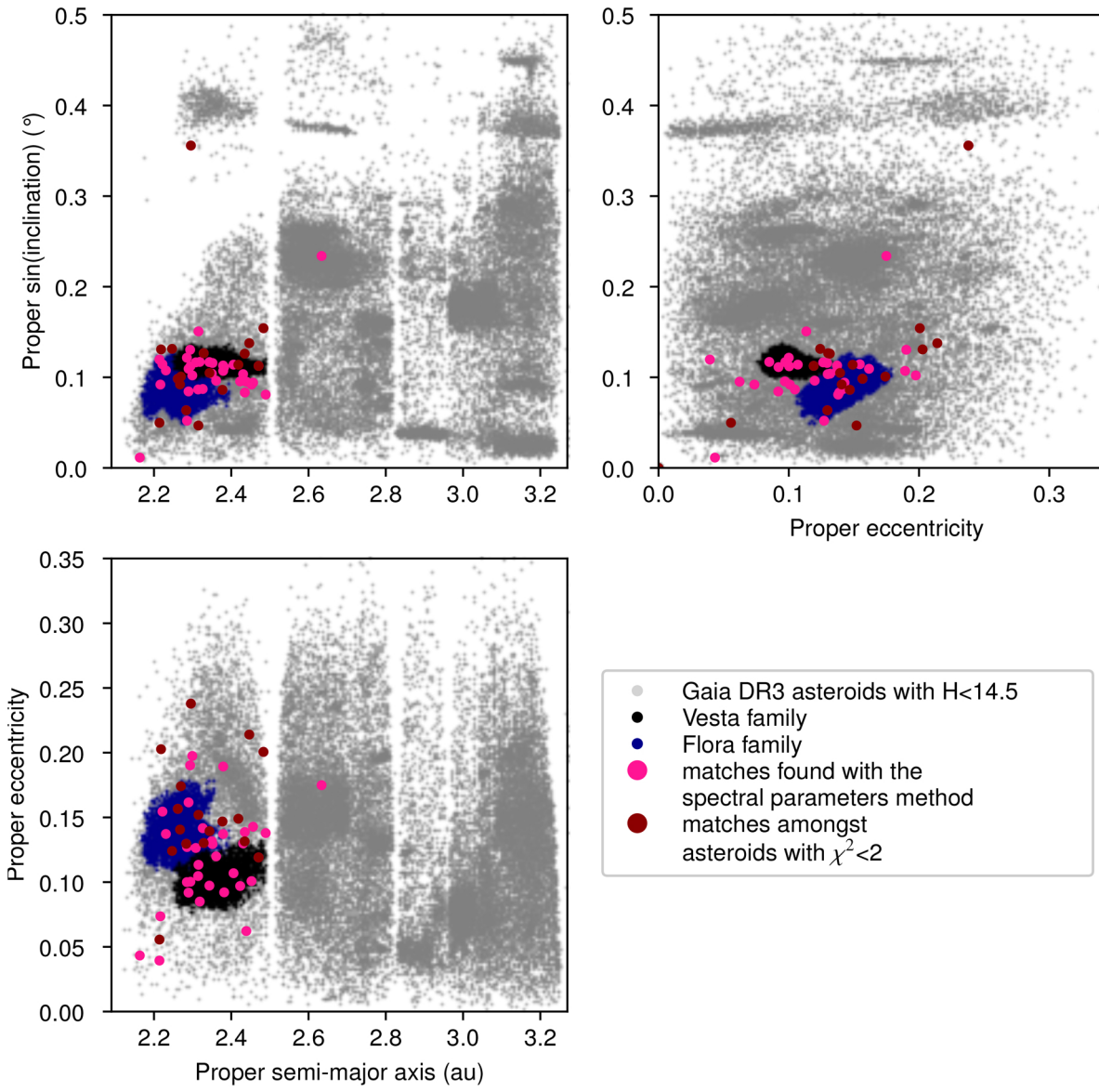

Fig. 5. Proper orbital element[1] plots of *Gaia* asteroids with absolute magnitude $H < 14.5$ (light grey dots). Vesta and Flora family members are indicated respectively with black and blue dots. Asteroids that were found to be spectroscopically matching with EC 002 after visual inspection are plotted with dots circles indicated in the legend above.

and meteorites (Nesvorný et al. 2002). The Flora family is mainly constituted of S-type asteroids (Oszkiewicz et al. 2015; Nesvorný et al. 2015, and references therein), which are linked to ordinary chondrites. Barrat et al. (2021) showed that EC 002 could be derived from the partial melt of a planetesimal of non-carbonaceous chondritic composition, which experienced heating during its accretion and consequently formed an igneous crust. If the asteroids belonging to the Flora family are (i) real EC 002 analogues, and (ii) true members of the Flora family, this would confirm the spectroscopic diversity within this family pointed out by several studies (Oszkiewicz et al. 2015, and references there in). In addition, this would potentially point towards a differentiation of the family parent body, as has been already proposed (Oszkiewicz et al. 2015).

Given the very low number of asteroids belonging to the other asteroid families, it is difficult to assume that the parent body of EC 002 was part of these families. Every other asteroids potentially matching with EC 002 do not belong to known families. However, current family catalogues are based on algorithms that determine the membership of an object to a family based on its proper orbital elements only, in order to distinguish the different families and to clearly identify their cores (Nesvorný et al. 2015; Tsirvoulis et al. 2018). As a result, some background objects are designated as family members but are in fact interlopers, and some real family members are not considered as part of the family, leading to halos of asteroids surrounding known families (Parker et al. 2008; Brož & Morbidelli 2013). In addition, the study of the dynamical behaviour of family and non-family asteroids by Dermott et al. (2018) lead to the conclusion that most asteroids in the inner main belt are or were originally part of the main known families, showing evidence that the families are very dispersed. Some of these dispersed families have been detected (Delbo et al. 2017, 2019) using the so-called V-shape method (Bolin et al. 2017), and more families are probably left to be identified (Delbo et al. 2017, 2019; Dermott et al. 2018).

[1] Data retrieved from the Belgrade catalogue http://asteroids.matf.bg.ac.rs/fam/properelements.php

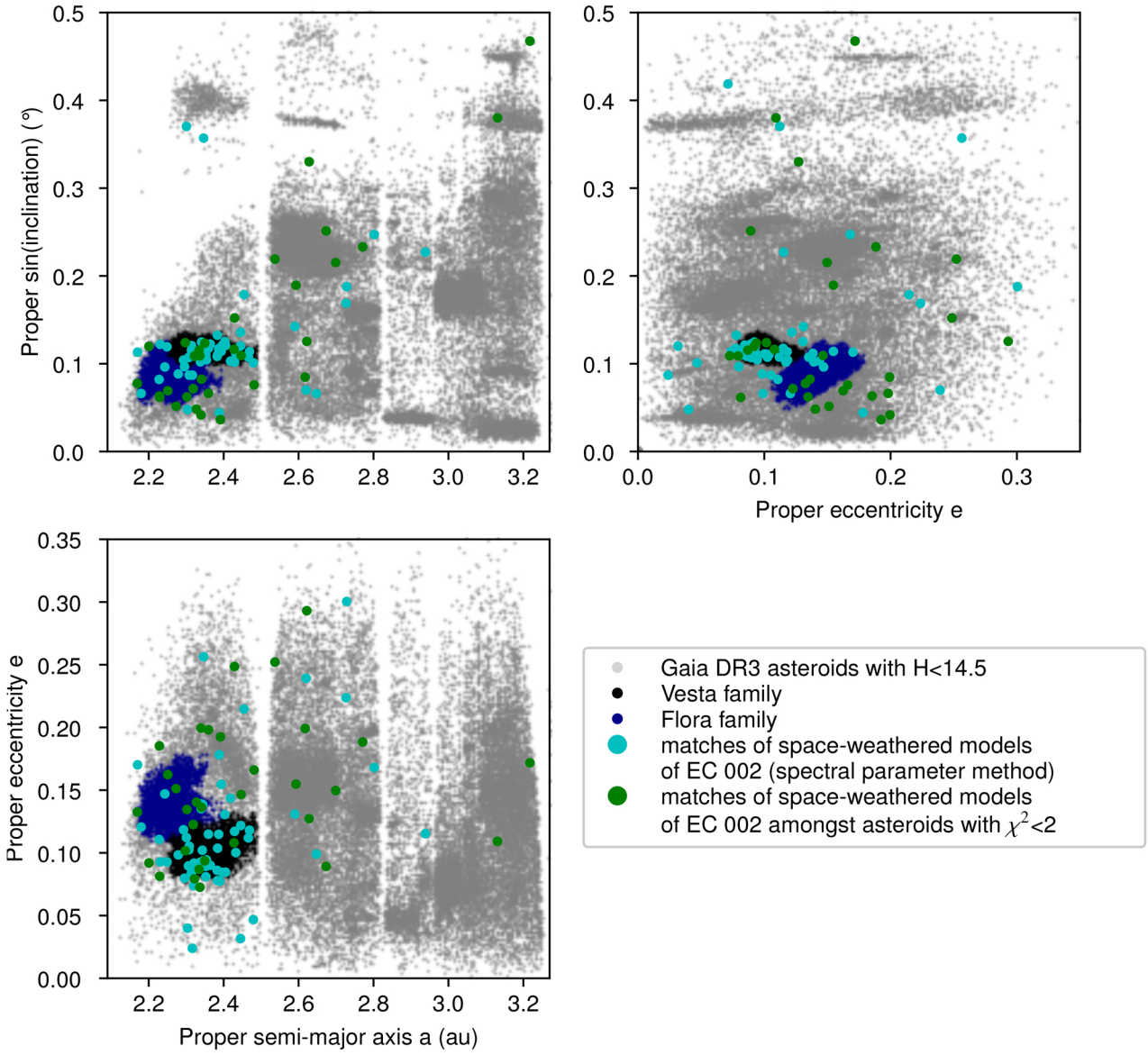

Fig. 6. Same as Fig. 5, but with cyan dots indicating asteroids that have spectral parameters compatible with the space-weathered models of EC 002 derived by Barrat et al. (2021) in the spectral parameters space. The green dots are asteroids matching the weathered models of the meteorite spectra using the curve matching method.

Hence, it is possible that the asteroids matching with EC 002 that are not listed as family members are part of very old families of the inner main belt that escaped identification up to now.

It is also established that laboratory spectra of meteorites do not necessarily match with the spectra of asteroids of analogue composition (Brunetto et al. 2015, and references therein). The reason is that the reflectance spectra of asteroids are affected by the exposure of their surface to weathering agents in space, such as solar wind ions and micrometeorites. Space weathering models have been developed, for example by Hapke (2001) or Brunetto et al. (2006), in order to correct reflectance spectra from space weathering. The Hapke model is based on the calculation of the absorption coefficient of a silicate host medium in which small nanophase iron spheres are included (see Brunetto et al. 2007, for further details). The inclusion of nanophase iron inside a siliceous material changes its physical properties and alters its visible and infrared spectrum: the spectral slope is reddened, the silicate bands become shallower and less recognisable and the albedo of the object is darkened. However, the silicate band centres are not (or very little) affected by this type of space weathering Gaffey et al. (2002). This model was developed by studying the space weathering of the Moon and it successfully recreates it. For its appliance to an object to be relevant, the mineralogy of the object needs to be dominated by silicates with grains larger than the wavelength (Pierre Beck, priv. comm.). Thus, the Hapke and other similar models (Brunetto et al. 2006) have been applied to ordinary chondrites and allowed to link this type of meteorites to S-type asteroids, giving precious information about the mineralogy of these asteroids. EC 002 is an achondrite with andesitic composition, corresponding to the partial melt of an ordinary chondrite and which contains silicates with large grains (Barrat et al. 2021). Therefore, using the Hapke model makes sense to simulate the effect of space weathering on an asteroid of the same composition as EC 002, as what was implemented by Barrat et al. (2021).

A characteristic feature of the EC 002 reflectance spectrum is the presence of an absorption band at 0.65 μm. Unfortunately, this feature cannot be used as an absolute diagnostic

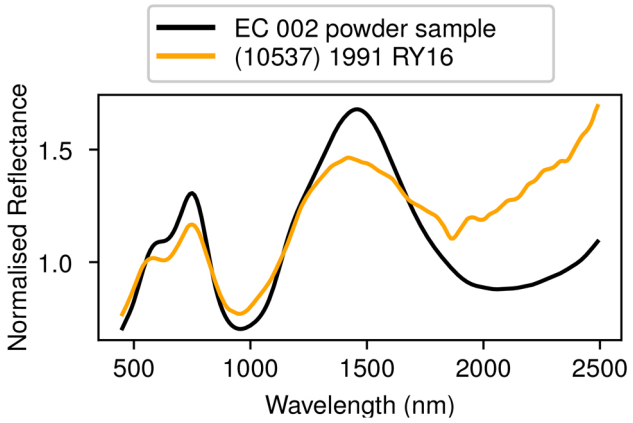

Fig. 7. VISNIR spectra of the powder sample of EC 002 (black lines) and of asteroid (10537) 1991 RY16 (orange lines) retrieved from Fig. 1 of Moskovitz et al. (2008). Both spectra were normalised at 550 nm. The two spectra show a similar shape, they both show a band around 0.65 µm and similar Band I centre. However their Band II centre is shifted with respect to each other.

feature in *Gaia* asteroid spectra for two reasons. First, the BP and RP spectra overlap in the region of this band. Since the spectrophotometers are independently calibrated (De Angeli et al. 2023), their overlapping region can be affected by artefacts (Gaia Collaboration 2023) and must be handled with care. The second reason is that some V-type asteroids also display an absorption band near 0.65 µm, such as the asteroid (10537) 1991 RY16 (Moskovitz et al. 2008). Interestingly, the visible reflectance spectra of asteroid (10537) 1991 RY16 and EC 002 are quite similar. This asteroid has already been found the closest match to the ungrouped achondrite (NWA) 7325 by Cloutis et al. (2018) based on the spectral features of both bodies, without being a satisfactory match. In the near-infrared however, EC 002 shows a deeper Band II depth and a Band II centre at longer wavelengths (1.89 µm for asteroid (10537) 1991 RY16, vs. 2.08 µm for EC 002, as visible Fig. 7). This points to the necessity of using near-infrared spectroscopy to distinguish potential EC 002 visible matches against V-type asteroids.

6. Conclusion and perspectives

We searched for analogues of the andesitic meteorite EC 002 among the asteroid population, using *Gaia* visible reflectance spectra. We studied four different laboratory samples of the meteorite: three raw slabs and one powder spectrum; and three modelled space-weathered spectra of EC 002 were also analysed. As first method, we evaluated and compared the spectral parameters of each sample of the meteorite with the ones of the asteroids, studying the slope and the Band I depth of each asteroid spectrum. The second method used was a curve matching method.

For both methods, a visual inspection of the asteroid spectra and a search in the literature for already existing VIS and NIR spectra of these objects allowed us to deduce which asteroids are the most probable analogues of EC 002 among the main-belt asteroid population. The spectral parameter method gave 41 objects as potential analogues to the laboratory samples of EC 002, and 70 objects matching the space-weathered spectra of EC 002. These objects are mostly located in the inner main belt, around the Vesta and Flora families.

The curve matching method gave 18 objects matching the laboratory samples of the meteorite, also concentrated in the inner main belt. The curve matching with the modelled space-weathered spectra of the meteorite gave 23 asteroids as potential analogues of the low space-weathered EC 002, eight asteroids matching the medium space-weathered meteorite and only one asteroid matching the highly space-weathered EC 002. Because of the $\chi^2_{\rm red}$ parameter used, only objects with a low S/N were found with this method. In the end, a total of 51 asteroids were found as potential analogues of the not-space-weathered EC 002, and 91 asteroids were found matching the modelled space-weathered spectra of the meteorite.

Finally, only 0.08% of *Gaia* asteroids were found to be matching the laboratory samples of the meteorite, and 0.15% were found matching the modelled space-weathered spectra. However, acquiring and studying the near-infrared spectra of these objects could help determining if they are real analogues of EC 002. If they are, they would be remnants of the original population of planetesimals that appeared in the early times of the Solar System and that showed an andesitic – and not basaltic – crust after differentiation. Traces of this original population would thus still exist in the main belt. Moreover, a full VISNIR spectrum would allow the study of more spectral parameters (Band II centre and band area ratio), which would give great clues about the quality of the matches presented in this work.

Acknowledgements. M.G. and M.D. acknowledge financial support from CNES and the Action Specifique *Gaia*. M.D., C.A., and L.G. acknowledge financial support from the ANR ORIGINS (ANR-18-CE31-0014). This work has made use of data from the European Space Agency (ESA) mission *Gaia* (`https://www.cosmos.esa.int/gaia`), processed by the *Gaia* Data Processing and Analysis Consortium (DPAC, `https://www.cosmos.esa.int/web/gaia/dpac/consortium`). Funding for the DPAC has been provided by national institutions, in particular the institutions participating in the *Gaia* Multilateral Agreement. This work is based on data provided by the Minor Planet Physical Properties Catalogue (MP3C) of the Observatoire de la Côte d'Azur. Spectra from Barrat et al. (2021) were used as well in this study. The authors are grateful to Jean-Alix Barrat and Pierre Beck for their precious help.

References

Alvarez-Candal, A., Duffard, R., Lazzaro, D., & Michtchenko, T. 2006, A&A, 459, 969
Arculus, R., Campbell, I. H., McLennan, S. M., & Taylor, S. R. 2009, Nature, 459, E1
Avdellidou, C., Delbo, M., Morbidelli, A., et al. 2022, A&A, 665, A9
Barrat, J.-A., Chaussidon, M., Yamaguchi, A., et al. 2021, Proc. Natl. Acad. Sci. USA, 118, 2026129118
Binzel, R. P., Xu, S., Bus, S. J., et al. 1993, Science, 262, 1541
Binzel, R. P., DeMeo, F. E., Turtelboom, E. V., et al. 2019, Icarus, 324, 41
Bland, P. A., Spurný, P., Towner, M. C., et al. 2009, Science, 325, 1525
Bolin, B. T., Delbo, M., Morbidelli, A., & Walsh, K. J. 2017, Icarus, 282, 290
Brož, M., & Morbidelli, A. 2013, Icarus, 223, 844
Brunetto, R., Vernazza, P., Marchi, S., et al. 2006, Icarus, 184, 327
Brunetto, R., de León, J., & Licandro, J. 2007, A&A, 472, 653
Brunetto, R., Loeffler, M. J., Nesvorný, D., Sasaki, S., & Strazzulla, G. 2015, in Asteroids IV, eds. P. Michel, F. E. DeMeo, & W. F. Bottke (University of Arizona Press), 597
Burbine, T. H., Buchanan, P. C., Binzel, R. P., et al. 2001, Meteor. Planet. Sci., 36, 761
Bus, S. J., & Binzel, R. P. 2002, Icarus, 158, 146
Carrasco, J. M., Weiler, M., Jordi, C., et al. 2021, A&A, 652, A86
Carry, B., Solano, E., Eggl, S., & DeMeo, F. E. 2016, Icarus, 268, 340
Carvano, J. M., Hasselmann, P. H., Lazzaro, D., & Mothé-Diniz, T. 2010, A&A, 510, A43
Chapman, C. R. 1986, in Proceedings of the NASA and CNR, International Workshop on Catastrophic Disruption of Asteroids and Satellites, 103
Cloutis, E. A. 2002, J. Geophys. Res. (Planets), 107, 5039
Cloutis, E. A., Reddy, V., & Blewett, D. T. 2018, Icarus, 311, 384
Collinet, M., & Grove, T. L. 2020, Geochim. Cosmochim. Acta, 277, 334

Day, J. M. D., Ash, R. D., Liu, Y., et al. 2009, Nature, 457, 179
De Angeli, F., Weiler, M., Montegriffo, P., et al. 2023, A&A, in press https://doi.org/10.1051/0004-6361/202243680
de Sanctis, M. C., Migliorini, A., Luzia Jasmin, F., et al. 2011, A&A, 533, A77
de Sanctis, M. C., Ammannito, E., Capria, M. T., et al. 2012, Science, 336, 697
Delbo, M., Walsh, K., Bolin, B., Avdellidou, C., & Morbidelli, A. 2017, Science, 357, 1026
Delbo, M., Avdellidou, C., & Morbidelli, A. 2019, A&A, 624, A69
DeMeo, F. E., & Carry, B. 2013, Icarus, 226, 723
DeMeo, F. E., Binzel, R. P., Slivan, S. M., & Bus, S. J. 2009, Icarus, 202, 160
DeMeo, F. E., Polishook, D., Carry, B., et al. 2019, Icarus, 322, 13
DeMeo, F. E., Burt, B. J., Marsset, M., et al. 2022, Icarus, 380, 114971
Dermott, S. F., Christou, A. A., Li, D., Kehoe, T. J. J., & Robinson, J. M. 2018, Nat. Astron., 2, 549
Gaffey, M. J., Cloutis, E. A., Kelley, M. S., & Reed, K. L. 2002, in Asteroids III, eds. W. F. Bottke, Jr., A. Cellino, P. Paolicchi, & R. P. Binzel (Tucson: University of Arizona Press), 183
Gaia Collaboration (Galluccio, L., et al.) 2023, A&A, in press, https://doi.org/10.1051/0004-6361/202243791
Granvik, M., Morbidelli, A., Jedicke, R., et al. 2016, Nature, 530, 303
Greenwood, R. C., Burbine, T. H., & Franchi, I. A. 2020, Geochim. Cosmochim. Acta, 277, 377
Hanuš, J., Delbo', M., Ďurech, J., & Alí-Lagoa, V. 2015, Icarus, 256, 101
Hanuš, J., Delbo, M., Durech, J., & Alí-Lagoa, V. 2018, Icarus, 309, 297
Hapke, B. 2001, J. Geophys. Res., 106, 10039
Hardersen, P. S., Reddy, V., Cloutis, E., et al. 2018, AJ, 156, 11
Harris, A. W., & Drube, L. 2014, ApJ, 785, L4
Henke, S., Gail, H. P., Trieloff, M., Schwarz, W. H., & Kleine, T. 2012, A&A, 545, A135
Ivezić, Ž., Tabachnik, S., Rafikov, R., et al. 2001, AJ, 122, 2749
Ivezic, Z., Juric, M., Lupton, R. H., Tabachnik, S., & Quinn, T. 2002, SPIE Conf. Ser., 4836, 98
Jasmim, F. L., Lazzaro, D., Carvano, J. M. F., Mothé-Diniz, T., & Hasselmann, P. H. 2013, A&A, 552, A85
Johansen, A., Jacquet, E., Cuzzi, J. N., Morbidelli, A., & Gounelle, M. 2015, in Asteroids IV, eds. P Michel, F. E. DeMeo, & W. F. Bottke (University of Arizona Press), 471
Jordi, C., Gebran, M., Carrasco, J. M., et al. 2010, A&A, 523, A48
Kryszczyńska, A. 2013, A&A, 551, A102
La Spina, A., Paolicchi, P., Kryszczyńska, A., & Pravec, P. 2004, Nature, 428, 400
Lazzaro, D., Angeli, C. A., Carvano, J. M., et al. 2004, Icarus, 172, 179
Leith, T. B., Moskovitz, N. A., Mayne, R. G., et al. 2017, Icarus, 295, 61
Lindsay, S. S., Marchis, F., Emery, J. P., Enriquez, J. E., & Assafin, M. 2015, Icarus, 247, 53
Lucas, M. P., Emery, J. P., MacLennan, E. M., et al. 2019, Icarus, 322, 227
Mahlke, M., Carry, B., & Mattei, P.-A. 2022, A&A, 665, A26
Mandler, B. E., & Elkins-Tanton, L. T. 2013, Meteor. Planet. Sci., 48, 2333
Mansour, J. A., Popescu, M., de León, J., & Licandro, J. 2020, MNRAS, 491, 5966
Matlovič, P., de Leon, J., Medeiros, H., et al. 2020, A&A, 643, A107
McCord, T. B., Adams, J. B., & Johnson, T. V. 1970, Science, 168, 1445
McSween, H. Y., J., Ghosh, A., Grimm, R. E., Wilson, L., & Young, E. D. 2002, in Asteroids III, eds. W. F. Bottke Jr., A. Cellino, P. Paolicchi, & R. P. Binzel (University of Arizona Press), 559
Medeiros, H., de León, J., Lazzaro, D., et al. 2019, MNRAS, 488, 3866
Migliorini, A., de Sanctis, M. C., Michtchenko, T. A., et al. 2021, MNRAS, 504, 2019
Morbidelli, A., Libourel, G., Palme, H., Jacobson, S. A., & Rubie, D. C. 2020, Earth Planet. Sci. Lett., 538, 116220
Morbidelli, A., Baillié, K., Batygin, K., et al. 2022, Nature Astronomy, 6, 72
Moskovitz, N. A., Jedicke, R., Gaidos, E., et al. 2008, Icarus, 198, 77
Moskovitz, N. A., Willman, M., Burbine, T. H., Binzel, R. P., & Bus, S. J. 2010, Icarus, 208, 773
Nesvorný, D., Morbidelli, A., Vokrouhlický, D., Bottke, W. F., & Brož, M. 2002, Icarus, 157, 155
Nesvorný, D., Bottke, W. F., Vokrouhlický, D., Morbidelli, A., & Jedicke, R. 2005, Proc. Int. Astron. Union, 1, 289
Nesvorný, D., Broz, M., & Carruba, V. 2015, in Asteroids IV, eds. P Michel, F. E. DeMeo, & W. F. Bottke (University of Arizona Press), 297
Oszkiewicz, D., Kankiewicz, P., Włodarczyk, I., & Kryszczyńska, A. 2015, A&A, 584, A18
Parker, A., Ivezić, Ž., Jurić, M., et al. 2008, Icarus, 198, 138
Popescu, M., Birlan, M., & Nedelcu, D. A. 2012, A&A, 544, A130
Popescu, M., Licandro, J., Carvano, J. M., et al. 2018, A&A, 617, A12
Ribeiro, A. O., Roig, F., Cañada-Assandri, M., et al. 2014, Planet. Space Sci., 92, 57
Righter, K., & Drake, M. J. 1997, Meteor. Planet. Sci., 32, 929
Russell, C. T., Raymond, C. A., Coradini, A., et al. 2012, Science, 336, 684
Russell, C. T., Raymond, C. A., Jaumann, R., et al. 2013, Meteor. Planet. Sci., 48, 2076
Ruzicka, A., Snyder, G. A., & Taylor, L. A. 1997, Meteor. Planet. Sci., 32, 825
Sanchez, J. A., Michelsen, R., Reddy, V., & Nathues, A. 2013, Icarus, 225, 131
Sergeyev, A. V., & Carry, B. 2021, A&A, 652, A59
Sergeyev, A. V., Carry, B., Onken, C. A., et al. 2022, A&A, 658, A109
Solontoi, M. R., Hammergren, M., Gyuk, G., & Puckett, A. 2012, Icarus, 220, 577
Trieloff, M., Hopp, J., & Gail, H.-P. 2022, Icarus, 373, 114762
Tsirvoulis, G., Morbidelli, A., Delbo, M., & Tsiganis, K. 2018, Icarus, 304, 14
Xu, S., Binzel, R. P., Burbine, T. H., & Bus, S. J. 1995, Icarus, 115, 1

Appendix A: Tables of asteroids matching the spectra of EC 002

Table A.1. Asteroids within the 'possible matches area'.

Asteroid	Acceptance	Notes	Type	Method	Ref.
(289) Nenetta	0	longer band I centre	A	Spec. VISNIR	5
(863) Benkoela	0	longer band I centre	A	Spec. VISNIR	5
(956) Elisa	0	-	V	Spec. VIS and NIR	3, 6
(1459) Magnya	0	VISNIR different	V	Spec. VISNIR	5
(1468) Zomba	0	NIR different	V	Spec. VISNIR	20
(1488) Aura	0	different red part	A	Phot. VIS	24
(1643) Brown	1	-	S	Phot. VIS	24
(1709) Ukraina	0	A type spectrum	A	Spec. VISNIR	25
(1908) Pobeda	0	longer band I centre	S	Phot. VIS	24
(1946) Walraven	1	-	V	Spec. VIS	4
(2168) Swope	0	-	V	Spec. NIR	16,22
(2371) Dimitrov	0	NIR different	V	Spec. VIS and NIR	2, 6
(2432) Soomana	1	-	V	Phot. VIS	10, 23
(2442) Corbett	0	shorter band I centre	V	Spec. VISNIR	5
(2557) Putnam	0	shorter band I centre	S	Phot. VIS	24
(2851) Harbin	0	-	V	Spec. VISNIR	5
(2912) Lapalma	0	-	V	Spec. VISNIR	5
(3104) Durer	0	different red part	K	Spec. VISNIR	25
(3155) Lee	0	shorter band I centre	V	Spec. VISNIR	5
(3188) Jekabsons	1	-	V	Spec. VIS	21
(3651) Friedman	1	bad two last points	V	Phot. VIS	24
(3817) Lencarter	0	shorter band I centre	-	-	-
(3869) Norton	1	article: related to 4 Vesta	V	Spec. VIS	1
(3882) Johncox	0	-	V	Spec. VISNIR	18
(4055) Magellan	0	-	V	Spec. VISNIR	5
(4088) Baggesen	1	no clear 0.65 μm band - SW low	-	-	-
(4302) Markeev	1	-	V	Phot. VIS	23
(4402) Tsunemori	0	different band I shape	A	Spec. VISNIR	25
(4692) SIMBAD	0	shorter band I centre	V	Phot. VIS	10, 23
(5037) Habing	0	shorter band I centre	V	Spec. VISNIR	25
(5121) Numazawa	1	-	S	Phot. VIS	24
(5498) Gustafsson	0	linked to howardites	V	Spec. VIS and NIR	6, 8
(5696) Ibsen	0	different red part			
(6003) 1988 VO1	1	SW low	X	Phot. VIS	24
(6046) 1991 RF14	0	shorter band I centre	V	Spec. VISNIR	18
(6159) Andreseloy	0	shorter band I centre	V	Spec. VISNIR	25
(6369) 1983 UC	0	shorter band I centre	-	-	-
(6584) Ludekpesek	0	shorter band I centre	V	Phot. NIR	17
(6728) 1991 UM	0	shorter band I centre	-	-	-
(6789) Milkey	1	SW low	-	-	-
(6853) Silvanomassaglia	1	-	V	Phot. NIR	17
(6876) Beppeforti	1	-	S	Phot. VIS	24, 24
(6877) Giada	0	shorter band I centre	V	Phot. NIR	17
(6964) Kunihiko	0	shorter band I centre	V	Phot. VIS	24
(7294) Barbaraakey	0	flatter red part	S	Phot. VIS	24
(7529) Vagnozzi	0	flatter red part	V	Phot. VIS	24
(7889) 1994 LX	0	noisy	V	Spec. VISNIR	20
(7933) Magritte	0	shorter band I centre	X	Phot. VIS	24
(7942) 1991 OK1	0	shorter band I centre	S	Phot. VIS	24
(8031) Williamdana	0	shorter band I centre	V	Phot. VIS	24
(8243) Devonburr	1	SW low	S	Phot. VIS	24, 24
(8483) Kinwalaniihsia	1	SW low (without first and last bands)	V	Phot. VIS	24
(8587) Ruficollis	1	-	K	Phot. VIS	24
(8660) Sano	0	longer band I centre	S	Phot. VIS	24
(8669) 1991 NS1	0	shorter band I centre	S	Phot. VIS	24
(8692) 1992 WH	1	SW low	S	Phot. VIS	24
(8827) Kollwitz	1	-	C	Phot. VIS	24
(8838) 1989 UW2	0	longer band I centre	A	Spec. VISNIR	19
(9115) Battisti	0	shorter band I centre	V	Phot. VIS	24
(9197) Endo	1	not very good VISNIR literature spectrum	V	Spec. VISNIR	22
(9432) Iba	0	shorter band I centre	V	Phot. VIS	24
(9433) 1997 CF3	1	-	C	Phot. VIS	24
(9593) 1991 PZ17	0	bump instead of 0.65 μm band	S	Phot. VIS	24
(9752) 1990 QZ1	0	longer band I centre	S	Phot. VIS	24

Table A.1. continued.

Asteroid	Acceptance	Notes	Type	Method	Ref.
(9753) 1990 QL3	1	SW low	-	-	-
(9974) Brody	1	SW high	-	-	-
(10156) 1994 VQ7	1	bad three last points	V	Phot. VIS	24
(10319) Toshiharu	0	shorter band I centre V	V	Phot. VIS	23, 24
(10418) 1998 WZ23	0	shorter band I centre	V	Phot. VIS	24
(10438) Ludolph	0	shorter band I centre	-	-	-
(10578) 1995 LH	0	bad BP RP overlapping	-	-	-
(10671) Mazurova	1	-	S	Phot. VIS	24
(10811) Lau	0	flatter red part	-	-	-
(10902) 1997 WB22	1	-	-	-	-
(11041) Fechner	0	shorter band I centre	V	Phot. VIS	7
(11155) Kinpu	1	-	S	Phot. VIS	24
(11764) Benbaillaud	0	shorter band I centre	V	Spec. VIS	8
(11861) Teruhime	0	longer band I centre	-	-	-
(11890) 1991 FF	0	longer band I centre	C	Phot. VIS	24
(11920) 1992 UY2	1	SW low (noisy)	C	Phot. VIS	24
(12551) 1998 QQ39	1	-	V	Phot. VIS	24
(12860) Turney	0	shorter band I centre	S	Phot. VIS	24, 24
(13133) Jandecleir	1	SW medium	S	Phot. VIS	24
(13704) Aletesi	0	shorter band I centre	C	Phot. VIS	24
(13714) Stainbrook	0	noisy	S	Phot. VIS	24
(13743) Rivkin	0	shorter band I centre	V	Phot. VIS	24
(13839) 1999 XF29	1	-	S	Phot. VIS	24
(14108) 1998 OA13	0	shorter band I centre	-	-	-
(14489) 1994 UW	0	-	V	Phot. VIS	23
(14511) Nickel	1	bump instead of band - SW low	-	-	-
(14562) 1997 YQ19	0	noisy	V	Spec VISNIR	25
(15031) Lemus	0	shorter band I centre	V	Phot. NIR	17
(15088) Licitra	1	SW low	S	Phot. VIS	24
(15759) 1992 GM4	0	shorter band I centre	V	Phot. VIS	24
(15989) 1998 XK39	1	-	V	Phot. VIS	24
(16866) 1998 AR	0	no clear band I	S	Phot. VIS	24
(16962) Elizawoolard	0	shorter band I centre	C	Phot. VIS	24
(17225) Alanschorn	0	shorter band I centre	-	-	-
(17240) Gletorrence	1	-	S	Phot. VIS	24
(17739) 1998 BY15	1	SW low	V	Phot. NIR	17
(17821) Bolsche	1	lower quality spectrum - SW low	C	Phot. VIS	24
(17882) Thielemann	1	SW low	V	Phot. VIS	24
(17904) Annekoupal	0	shorter band I centre	S	Phot. VIS	24
(17943) 1999 JZ6	1	SW low	V	Phot. VIS	24
(17951) Fenska	0	shorter band I centre	-	-	-
(18102) Angrilli	0	shorter band I centre	-	-	-
(18143) 2000 OK48	1	SW medium	A	Phot. VIS	10, 23, 24
(18280) 4245 T-3	0	more similar to a V type	S	Phot. VIS	24
(18344) 1989 TN11	1	SW low	V	Phot. VIS	24
(19230) Sugazi	0	shorter band I centre	V	Phot. NIR	17
(19281) 1996 AP3	0	-	V	Spec. VISNIR	18
(19487) Rosscoleman	0	shorter band I centre	-	-	-
(19589) Kirkland	0	noisy	V	Phot. VIS	24
(19754) Paclements	1	SW high or medium	S	Phot. VIS	10, 23, 24
(19978) 1989 TN6	1	SW low	V	Phot. VIS	10, 23
(20079) 1994 EP	0	shorter band I centre	V	Phot. VIS	24
(20157) 1996 TS18	0	shorter band I centre	S	Phot. VIS	24
(20237) Clavius	0	no clear band I	-	-	-
(20289) Nettimi	1	SW low (noisy)	-	-	-
(20454) Pedrajo	1	noisy	S	Phot. VIS	24
(20955) 2387 T-3	0	shorter band I centre	S	Phot. VIS	24
(21318) 1996 XU26	1	SW low	-	-	-
(21435) Aharon	0	noisy	-	-	-
(21891) Andreabocelli	0	shorter band I centre	-	-	-
(22113) 2000 RH9	0	shorter band I centre	V	Phot. VIS	10, 23
(22197) 3555 P-L	0	shorter band I centre	C	Phot. VIS	24
(22322) Bodensee	0	shorter band I centre	V	Phot. VIS	24
(23306) Adamfields	0	shorter band I centre	S	Phot. VIS	24
(23502) 1992 DE3	0	shorter band I centre	-	-	-
(23595) 1995 VR11	0	shorter band I centre	C	Phot. VIS	24
(23766) 1998 MZ23	1	SW low	S	Phot. VIS	24
(24286) 1999 XU188	1	-	S	Phot. VIS	24

Table A.1. continued.

Asteroid	Acceptance	Notes	Type	Method	Ref.
(24569) 9609 P-L	1	SW low or medium	S	Phot. NIR	17
(24684) 1990 EU4	1	SW low	S	Phot. NIR	17
(24892) 1997 AD3	1	-	-	-	-
(25434) Westonia	0	shorter band I centre	V	Phot. VIS	23, 24
(25752) 2000 BE8	0	noisy + bad BP-RP alignment	-	-	-
(25808) 2000 CK103	0	flatter red part	S	Phot. VIS	24
(26084) 1981 EK17	1	SW low	S	Phot. VIS	24
(26417) Michaelgord	0	bad BP-RP overlapping	V	Phot. VIS	10, 23, 24
(26573) 2000 EG87	1	-	V	Phot. VIS	24
(26851) Sarapul	1	SW low	-	-	-
(27106) Jongoldman	0	shorter band I centre	V	Phot. VIS	24
(27162) 1999 AM6	0	shorter band I centre	S	Phot. VIS	24
(27262) 1999 XT184	1	bad RP	X	Phot. VIS	24
(27390) Kyledavis	0	shorter band I centre	-	-	-
(27399) Gehring	0	shorter band I centre	C	Phot. VIS	24
(27876) 1996 BM4	1	SW low	S	Phot. VIS	24
(27884) 1996 EZ1	1	SW low	S	Phot. VIS	24
(28132) Karenzobel	1	SW low	S	Phot. VIS	24
(28162) 1998 VD14	1	-	-	-	-
(28291) 1999 CX52	0	shorter band I centre	V	Spec. VIS	9
(29171) 1990 QK3	1	bump instead of 0.65 μm band - SW low	-	-	-
(29269) 1993 FD25	0	shorter band I centre	C	Phot. VIS	24
(30426) Philtalbot	1	SW low	V	Phot. VIS	23
(30751) 1981 EL29	0	shorter band I centre	S	Phot. VIS	24
(30769) 1984 ST2	1	-	-	-	-
(30781) 1988 CR2	0	shorter band I centre	C	Phot. VIS	24
(30820) 1990 RU2	0	more similar to a V type	S	Phot. VIS	24
(30834) 1990 VR6	1	SW low	V	Phot. VIS	10, 23
(30892) 1993 FR18	0	shorter band I centre	A	Phot. VIS	23
(31060) 1996 TB6	1	SW medium	SQ	Phot. VIS	7
(31414) Rotarysusa	0	shorter band I centre	V	Spec. VISNIR	25
(31544) 1999 DZ5	0	shorter band I centre	V	Phot. VIS	24
(31572) 1999 FM22	0	shorter band I centre	V	Phot. VIS	24
(31622) 1999 GL19	0	shorter band I centre	-	-	-
(32168) 2000 NP9	0	shorter band I centre	-	-	-
(32449) Crystalmiller	0	shorter band I centre	S	Phot. VIS	24
(32590) Cynthiachen	0	shorter band I centre SW low	V	Phot. VIS	10, 23
(33418) Jacksonweaver	1	-	V	Phot. VIS	10, 23
(33562) Amydunphy	0	different red part	V	Phot. NIR	17
(33881) 2000 JK66	0	-	V	Spec. VISNIR	20
(33947) 2000 ML1	1	SW low	S	Phot. VIS	24
(34698) 2001 OD22	0	shorter band I centre	V	Spec. NIR	16
(34706) 2001 OP83	0	Vesta family	V	Spec. NIR	14
(35193) 1994 CG14	0	no clear band I	C	Phot. VIS	24
(35364) Donaldpray	1	SW low	V	Phot. VIS	10
(36360) 2000 OH3	0	shorter band I centre	S	Phot. VIS	24
(36363) 2000 OB5	0	shorter band I centre	S	Phot. VIS	24
(36431) 2000 PJ12	1	-	V	Phot. VIS	7
(36798) 2000 SA43	0	shorter band I centre + noisy	S	Phot. VIS	24
(37306) 2001 KW46	0	no clear band I	-	-	-
(37386) 2001 WG29	0	shorter band I centre	V	Phot. NIR	17
(39940) 1998 FR99	1	SW low (bad BP)	-	-	-
(40056) 1998 KT44	0	shorter band I centre	C	Phot. VIS	24
(41574) 2000 SQ1	0	no clear band I	-	-	-
(41765) 2000 VV35	0	shorter band I centre	X	Phot. VIS	24
(41894) 2000 WH121	1	SW low	-	-	-
(42644) 1998 FE67	0	bump instead of 0.65 μm band	V	Phot. NIR	17
(42822) 1999 NT13	1	SW medium	S	Phot. VIS	24, 24
(43278) 2000 ES109	1	SW low	C	Phot. VIS	24
(43302) 2000 GE114	0	shorter band I centre	V	Phot. VIS	24
(43388) 2000 WA61	0	shorter band I centre	V	Phot. NIR	17
(44150) 1998 HC108	1	-	V	Phot. VIS	10, 23
(44162) 1998 HC148	1	SW low	C	Phot. VIS	24
(44322) 1998 RZ42	1	SW medium	S	Phot. VIS	24
(44711) Carp	0	no clear band I	S	Phot. VIS	24
(44940) 1999 VH53	0	shorter band I centre	C	Phot. VIS	24, 24
(45417) 2000 AZ151	0	shorter band I centre	-	-	-
(45787) 2000 OJ24	1	SW low	-	-	-

Table A.1. continued.

Asteroid	Acceptance	Notes	Type	Method	Ref.
(46701) Interrante	0	shorter band I centre	V	Phot. VIS	23
(47232) 1999 VQ36	1	good agreement between 500 and 950 nm	C	Phot. VIS	24
(47398) 1999 XC116	0	bump instead of 0.65 μm band	V	Phot. VIS	23
(47463) 1999 XE258	0	shorter band I centre	-	-	-
(48039) 2001 DT69	1	SW low	V	Phot. VIS	23
(48114) 2001 FW77	0	different blue part	S	Phot. VIS	10, 23
(48323) 2002 NN33	0	low quality spectrum	S	Phot. VIS	24
(48632) 1995 SV29	0	more similar to a V type	V	Phot. VIS	10
(49101) 1998 RE76	1	-	V	Phot. VIS	10, 23
(49141) 1998 SM41	1	SW medium (or A type?)	A	Phot. VIS	10, 23
(49901) 1999 XK164	0	shorter band I centre	S	Phot. VIS	24
(50139) 2000 AH129	0	no clear band I	-	-	-
(50236) 2000 BB3	0	shorter band I centre SW low	V	Phot. VIS	24
(51379) 2001 BY7	1	SW medium (noisy)	C	Phot. VIS	24
(51443) 2001 FN27	0	bump instead of band	V	Phot. NIR	17
(51659) Robohachi	1	SW low (noisy)	S	Phot. VIS	24
(52216) 5014 T-3	0	shorter band I centre	V	Phot. VIS	24
(52408) 1993 TJ34	1	SW medium	-	-	-
(52995) 1998 UJ32	0	shorter band I centre	V	Phot. NIR	17
(53417) 1999 NP38	1	SW low	-	-	-
(53425) 1999 SO4	0	noisy	S	Phot. VIS	10, 23
(53593) 2000 CJ58	0	shorter band I centre	S	Phot. VIS	24
(53661) 2000 DU62	1	SW low	S	Phot. VIS	24
(53899) 2000 FM49	1	SW low or medium	-	-	-
(54061) 2000 GX134	0	shorter band I centre	-	-	-
(55549) 2001 XC59	1	noisy but plausible	S	Phot. VIS	24
(55831) 1995 XL	0	bad BP-RP alignment	S	Phot. NIR	17
(56348) 2000 AH69	0	shorter band I centre	C	Phot. VIS	24
(56561) Jaimenomen	1	SW low	-	-	-
(56585) 2000 JZ29	0	shorter band I centre	Q	Phot. VIS	24
(56696) 2000 LQ26	0	shorter band I centre	V	Phot. VIS	10, 23
(56904) 2000 QP171	1	-	C	Phot. VIS	24
(57857) 2001 XJ203	0	shorter band I centre	-	-	-
(58640) 1997 WH18	1	SW low	-	-	-
(59228) 1999 CH	0	shorter band I centre	V	Phot. VIS	10, 23
(59530) 1999 JU24	0	shorter band I centre	-	-	-
(59686) 1999 JS108	0	shorter band I centre	-	-	-
(60285) 1999 XR106	0	shorter band I centre	S	Phot. VIS	24
(60584) 2000 EW132	0	shorter band I centre	S	Phot. VIS	24
(61098) 2000 LY28	1	SW low	V	Phot. VIS	24
(61203) 2000 OY4	0	-	V	Phot. VIS	24
(61682) 2000 QV124	0	shorter band I centre	C	Phot. VIS	24
(63366) 2001 HK4	0	different red part	V	Phot. VIS	10
(63438) 2001 MY28	0	no clear band I	-	-	-
(64252) 2001 TL168	0	shorter band I centre	A	Phot. VIS	24
(64458) 2001 VF35	1	SW low	V	Phot. NIR	17
(64948) 2001 YH124	0	noisy	S	Phot. VIS	24
(65707) 1992 PY1	0	bad quality spectrum	-	-	-
(66679) 1999 TD29	0	shorter band I centre	V	Phot. VIS	24
(68765) 2002 EE99	0	shorter band I centre	-	-	-
(69595) 1998 FK11	0	shorter band I centre	V	Phot. VIS	24
(69628) 1998 FD62	0	shorter band I centre	S	Phot. VIS	24
(74107) 1998 QM37	1	SW low? Bad BP-RP overlapping?	-	-	-
(75323) 1999 XY47	1	SW low	-	-	-
(75441) 1999 XB129	0	shorter band I centre	S	Phot. VIS	24
(77584) 2001 KP14	0	noisy	S	Phot. VIS	24
(77590) 2001 KM17	0	shorter band I centre	V	Phot. NIR	17
(78034) 2002 JF82	0	shorter band I centre	V	Phot. VIS	7
(79137) 1991 PD15	0	no band I	-	-	-
(80356) 1999 XM124	0	no clear band I	Ad	Phot. NIR	17
(80863) 2000 DT27	0	more similar to a V type	V	Phot. VIS	10
(85301) 1994 UM5	0	shorter band I centre	-	-	-
(87093) 2000 LW6	1	-	V	Phot. VIS	23
(87216) 2000 OG38	1	SW low (bad BP spectrum)	-	-	-
(88912) 2001 TS8	0	no clear band I	V	Phot. VIS	24
(88955) 2001 TW42	1	-	S	Phot. VIS	24
(89776) 2002 AL90	1	SW low	-	-	-
(89952) 2002 JB20	1	SW low	S	Phot. VIS	24

Table A.1. continued.

Asteroid	Acceptance	Notes	Type	Method	Ref.
(90604) 4813 P-L	1	bad red part	S	Phot. VIS	24
(90843) 1995 YZ22	1	SW medium	-	-	-
(90855) 1996 GZ8	0	bump instead of band	C	Phot. VIS	24
(91343) 1999 JP30	0	shorter band I centre	V	Phot. NIR	17
(92593) 2000 PN16	1	SW low	-	-	-
(98482) 2000 UL101	0	noisy	S	Phot. VIS	24
(98745) 2000 YB47	0	shorter band I centre	V	Phot. NIR	17
(99714) 2002 JQ41	1	SW medium	S	Phot. VIS	24
(102071) 1999 RK139	0	shorter band I centre	V	Phot. VIS	10, 23
(102107) 1999 RL164	0	shorter band I centre	V	Phot. VIS	10
(102195) 1999 ST10	0	noisy	-	-	-
(102469) 1999 TC237	0	bap BP RP overlapping?	V	Phot. VIS	23
(108139) 2001 GL11	1	SW low	V	Phot. VIS	7
(108199) 2001 HX21	0	no clear band I	-	-	-
(112326) 2002 MM4	1	SW low	V	Phot. VIS	23
(114486) 2003 AJ57	0	-	-	-	-
(119385) 2001 TU7	0	bump instead of 0.65 μm band, bad blue and red parts	V	Phot. NIR	17
(122122) 2000 JM16	1	SW low	V	Phot. VIS	23
(122125) 2000 JO17	1	SW medium	S	Phot. VIS	10, 23
(125002) 2001 TJ154	0	shorter band I centre	-	-	-
(127422) 2002 OX11	0	low quality spectrum	S	Phot. VIS	10, 23
(128450) 2004 NX24	1	SW low	-	-	-
(130988) 2000 WT141	0	NEA	V	Spec. VIS	13
(133245) 2003 RL2	0	shorter band I centre	-	-	-
(134693) 1999 XP67	0	noisy	-	-	-
(134916) 2000 YP53	1	bad RP spectrum, SW low	-	-	-
(149372) 2002 XC71	0	bad agreement before 700 nm	-	-	-
(150544) 2000 SG164	0	noisy	X	Phot. VIS	23
(158242) 2001 TM24	0	bad BP-RP alignment	V	Phot. VIS	23
(163804) 2003 QQ88	0	noisy	S	Phot. VIS	7
(179587) 2002 LS2	0	-	S	Phot. VIS	15
(180757) 2004 NE33	0	-	-	-	-
(190138) 2005 RW27	0	shorter band I centre	-	-	-
(190664) 2000 YX90	0	bad BP-RP overlapping	-	-	-
(205560) 2001 SC282	1	noisy but plausible	-	-	-
(230762) 2003 WP192	1	SW medium	-	-	-
(310436) 2000 AB169	1	noisy but plausible	-	-	-

Note: The information in the table are the number and name of the 305 asteroids, if they are accepted or not as a match for EC 002 (1 if accepted, 0 if not), some notes about the visual inspection, the spectral type of the asteroid if determined and the method and relevant references associated (Ref column). The taxonomic scheme used for the type of each asteroid is the one used in the reference papers associated. Spec. stands for Spectroscopy and Phot. for Photometry.

Table A.2. Asteroids found as a match to the powder and raw slab samples of EC 002 with a curve-matching method.

Asteroid	Acceptance	Notes	Type	Method	Ref.
(6853) Silvanomassaglia	1	-	V	Phot. NIR	17
(10156) 1994 VQ7	1	-	V	Phot. VIS	24
(13743) Rivkin	0	shorter band I centre	V	Phot. VIS	24
(16856) Banach	1	-	S	Phot. VIS	24
(17056) Boschetti	1	-	S	Phot. VIS	24
(20289) Nettimi	0	noisy and unclear band I	-	-	-
(20454) Pedrajo	1	-	S	Phot. VIS	24
(23522) 1992 WC9	0	shorter band I centre	V	Phot. NIR	17
(24143) 1999 VY124	0	noisy	C	Phot. VIS	24
(24892) 1997 AD3	1	-	-	-	-
(26399) Rileyennis	0	shorter band I centre	-	-	-
(26420) 1999 XL103	0	shorter band I centre	V	Phot. VIS	23
(27106) Jongoldman	0	shorter band I centre	V	Phot. VIS	24
(27627) 2038 P-L	0	shorter band I centre	V	Phot. VIS	24
(30000) Camenzind	0	shallow slope	V	Phot. VIS	10, 23, 24
(30081) Zarinrahman	0	shorter band I centre	S	Phot. VIS	24
(38690) 2000 QS29	0	unclear band I	S	Phot. VIS	24
(40693) 1999 RX229	0	unclear band I	C	Phot. VIS	24
(44691) 1999 RF221	0	shallow slope	C	Phot. VIS	24
(47327) 1999 XZ25	0	shorter band I centre	V	Phot. VIS	10, 23
(48632) 1995 SV29	0	shorter band I centre	V	Phot. VIS	10
(50488) 2000 DA86	0	shallow slope	-	-	-
(51659) Robohachi	0	noisy	S	Phot. VIS	24

Table A.2. continued.

Asteroid	Acceptance	Notes	Type	Method	Ref.
(51688) 2001 KW12	0	shorter band I centre	S	Phot. VIS	24
(53561) 2000 CM22	0	noisy and unclear band I	S	Phot. VIS	24
(54062) 2000 GX135	1	noisy but plausible	C	Phot. VIS	24
(55549) 2001 XC59	1		S	Phot. VIS	24
(55866) 1997 PV4	0	shallow slope	V	Phot. VIS	24
(59686) 1999 JS108	0	shorter band I centre	-	-	-
(61169) 2000 NY20	0	band red and blue parts	X	Phot. VIS	24
(63653) 2001 QQ109	1	-	-	-	-
(64181) 2001 TS64	0	shorter band I centre	V	Phot. VIS	23
(68814) 2002 GP66	0	shallow slope	-	-	-
(77147) 2001 EV6	1	bad two last points	S	Phot. VIS	24
(77590) 2001 KM17	0	shorter band I centre	V	Phot. NIR	17
(77935) 2002 GM54	1	noisy but plausible	V	Phot. VIS	24
(78034) 2002 JF82	0	shorter band I centre	V	Phot. VIS	7
(80924) 2000 DJ73	0	noisy and unclear band I	C	Phot. VIS	24
(81448) 2000 GV123	0	shallow slope	S	Phot. VIS	24
(87010) 2000 JR55	0	shallow slope	C	Phot. VIS	24, 24
(88955) 2001 TW42	1	-	S	Phot. VIS	24
(89556) 2001 XS98	1	except for last points	-	-	-
(93893) 2000 WL141	0	unclear band I	S	Phot. VIS	10, 23, 24
(96353) 1997 VF3	0	flatter spectrum	C	Phot. VIS	24
(99722) 2002 JW46	0	flatter spectrum	S	Phot. VIS	24
(102107) 1999 RL164	0	shorter band I centre	V	Phot. VIS	10
(103308) 2000 AH55	0	unclear band I	-	-	-
(119144) 2001 PH32	0	unclear band I	V	Phot. VIS	10, 23
(123113) 2000 SH361	1	-	V	Phot. VIS	23
(124884) 2001 TE41	1	-	V	Phot. VIS	10, 23
(130988) 2000 WT141	0	NEA	V	Spec. VIS	13
(147124) 2002 TH129	0	less pronounced band	-	-	-
(149372) 2002 XC71	0	bad agreement before 700 nm	-	-	-
(153408) 2001 QV137	0	shorter band I centre	-	-	-
(164121) 2003 YT1	1	RP noisy but plausible	V	Spec. VISNIR	12
(194248) 2001 TA199	0	flatter spectrum	-	-	-
(205560) 2001 SC282	1	noisy but plausible	-	-	-
(310436) 2000 AB169	1	noisy but plausible	-	-	-

Note: The information in the table are the number and name of the 58 asteroids, if they are accepted or not as a good match for EC 002 (1 if accepted, 0 if not), some notes about the visual inspection, the spectral type of the asteroid if determined and the method and relevant references associated (Ref. column). The taxonomic scheme used for the type of each asteroid is the one used in the reference papers associated. Spec. stands for Spectroscopy and Phot. for Photometry.

Note: The references are (1) Xu et al. (1995), (2) Bus & Binzel (2002), (3) Lazzaro et al. (2004), (4) Alvarez-Candal et al. (2006), (5) DeMeo et al. (2009), (6) Moskovitz et al. (2010), (7) Carvano et al. (2010), (8) de Sanctis et al. (2011), (9) Solontoi et al. (2012), (10) DeMeo & Carry (2013), (11) Jasmim et al. (2013), (12) Sanchez et al. (2013), (13) Ribeiro et al. (2014), (14) Lindsay et al. (2015), (15) Carry et al. (2016), (16) Hardersen et al. (2018), (17) Popescu et al. (2018), (18)Medeiros et al. (2019), (19) DeMeo et al. (2019), (20) Binzel et al. (2019), (21) Matlovič et al. (2020), (22) Migliorini et al. (2021), (23) Sergeyev & Carry (2021), (24) Sergeyev et al. (2022), (25) Mahlke et al. (2022)

Table A.3. Accepted asteroids as candidate matches to the three space-weathered modelled samples of EC 002.

Asteroid	Type	Method	Ref
SW low			
(10131) Stanga	S	Phot. VIS	24
(15623) 2000 HU30	S	Phot. NIR	17
(18780) Kuncham	S	Phot. VIS	24
(20535) Marshburrows	L	Phot. VIS	24
(22276) Belkin	S	Phot. VIS	24
(22538) Lucasmoller	S	Phot. VIS	24
(24684) 1990 EU4	S	Phot. NIR	17
(27876) 1996 BM4	S	Phot. VIS	24
(32835) 1992 EO5	V	Phot. VIS	24
(33423) 1999 DK	A	Phot. VIS	23
(33852) Baschnagel	V	Phot. VIS	24
(33934) 2000 LA30	S	Phot. VIS	24
(33947) 2000 ML1	S	Phot. VIS	24
(43278) 2000 ES109	C	Phot. VIS	24
(56561) Jaimenomen	-	-	-
(65504) 3544 P-L	V	Phot. NIR	17
(74378) 1998 XH11	S	Phot. NIR	17
(79827) 1998 WU3	-	-	-
(89952) 2002 JB20	S	Phot. VIS	24
(100440) 1996 PJ6	-	-	-
(103308) 2000 AH55	-	-	-
(108139) 2001 GL11	V	Phot. VIS	7
(112326) 2002 MM4	V	Phot. VIS	23
SW medium			
(42822) 1999 NT13	S	Phot. VIS	24
(44322) 1998 RZ42	S	Phot. VIS	24
(68089) 2000 YS108	-	-	-
(68946) 2002 PX138	S	Phot. VIS	24
(93797) 2000 WO43	S	Phot. VIS	10
(108899) 2001 PP5	-	-	-
(145532) 2006 FD42	-	-	-
(230762) 2003 WP192	-	-	-
SW high			
(33809) 1999 XK152	C	Phot. VIS	24

Note: This selection has been done after visual inspection of 269 asteroids for the low space-weathered sample, 223 asteroids for the medium space weathering and 12 asteroids for the high space weathering. The references associated with the numbers in the Ref. column are given in appendix. The taxonomic scheme used for the type of each asteroid is the one used in the reference papers associated. SW stands for space weathering.

Appendix B: Spectra of the asteroids matching the spectra of EC 002

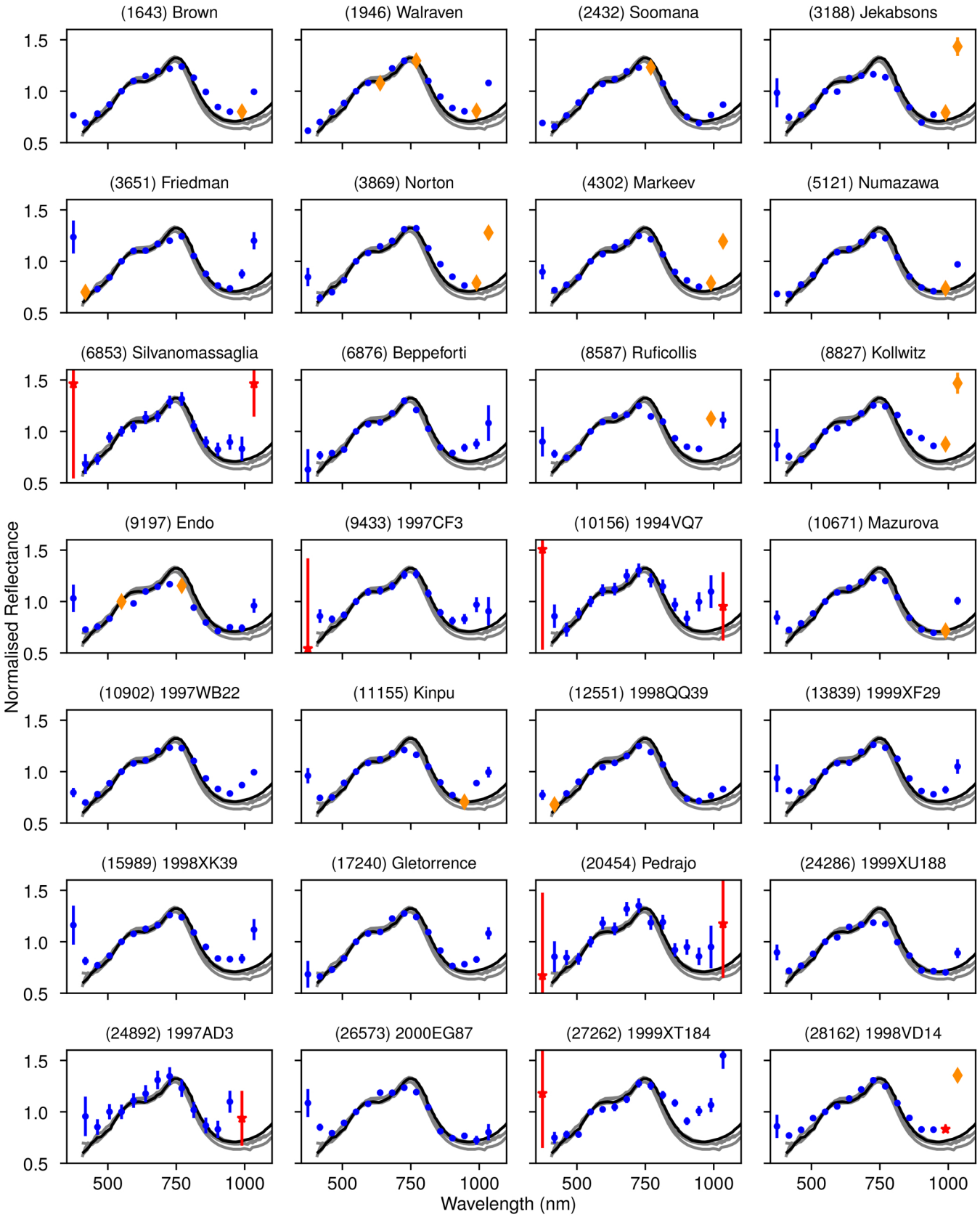

Fig. B.1. Spectra of the 41 asteroids found in the 'possible matches area', validated as matches of EC 002 after visual inspection. The spectra are normalised at 550 nm. Black continuous line: spectrum of the powder sample of the meteorite, grey lines: spectra of the raw slab samples. The 16 bands of the Gaia asteroid spectra are given a colour and a symbol according to the value of the flag associated to the band: blue circle if flag=0, orange diamond if flag=1 and red star if flag=2. This way of showing the asteroid spectra applies for every figure hereafter.

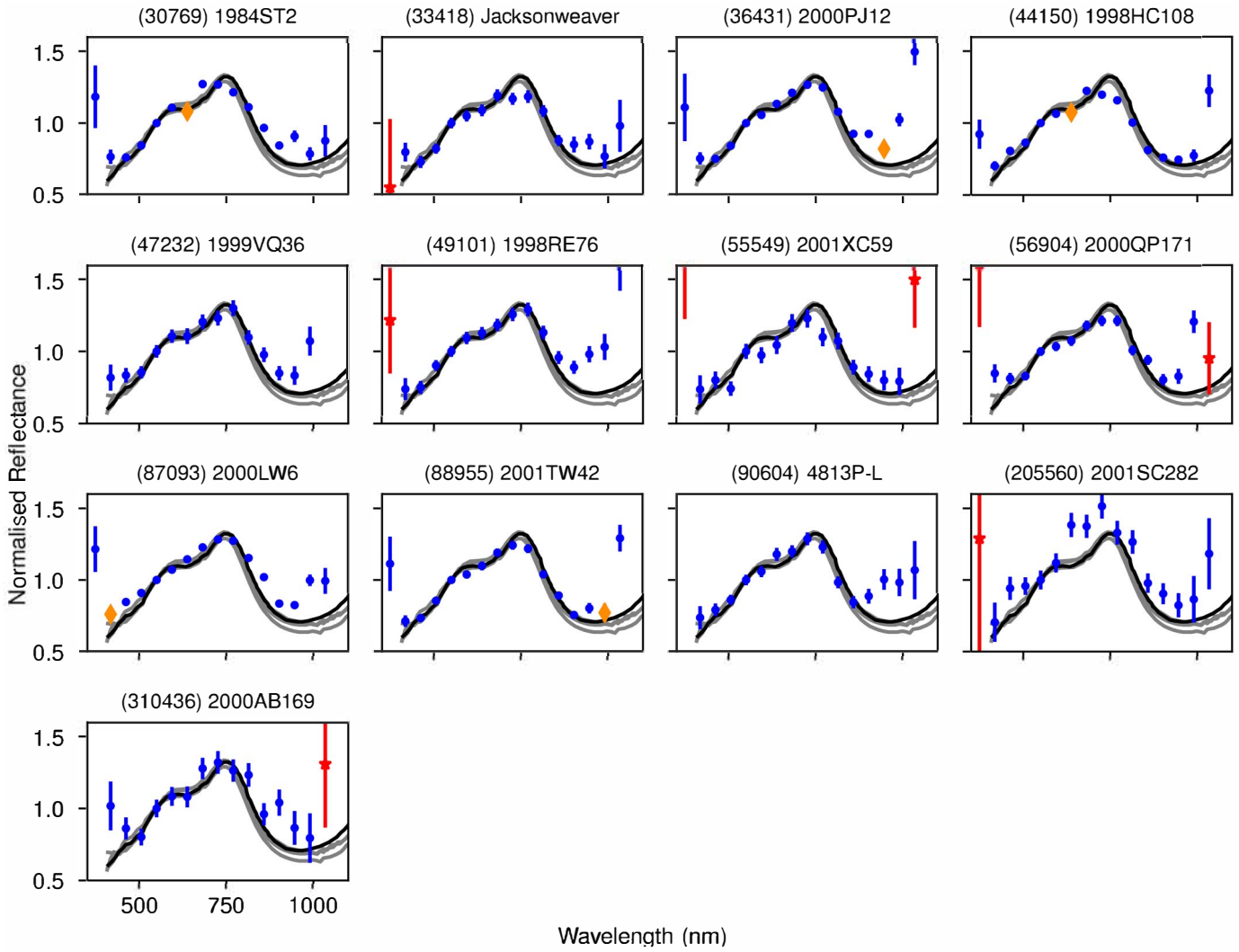

Fig. B.1. continued.

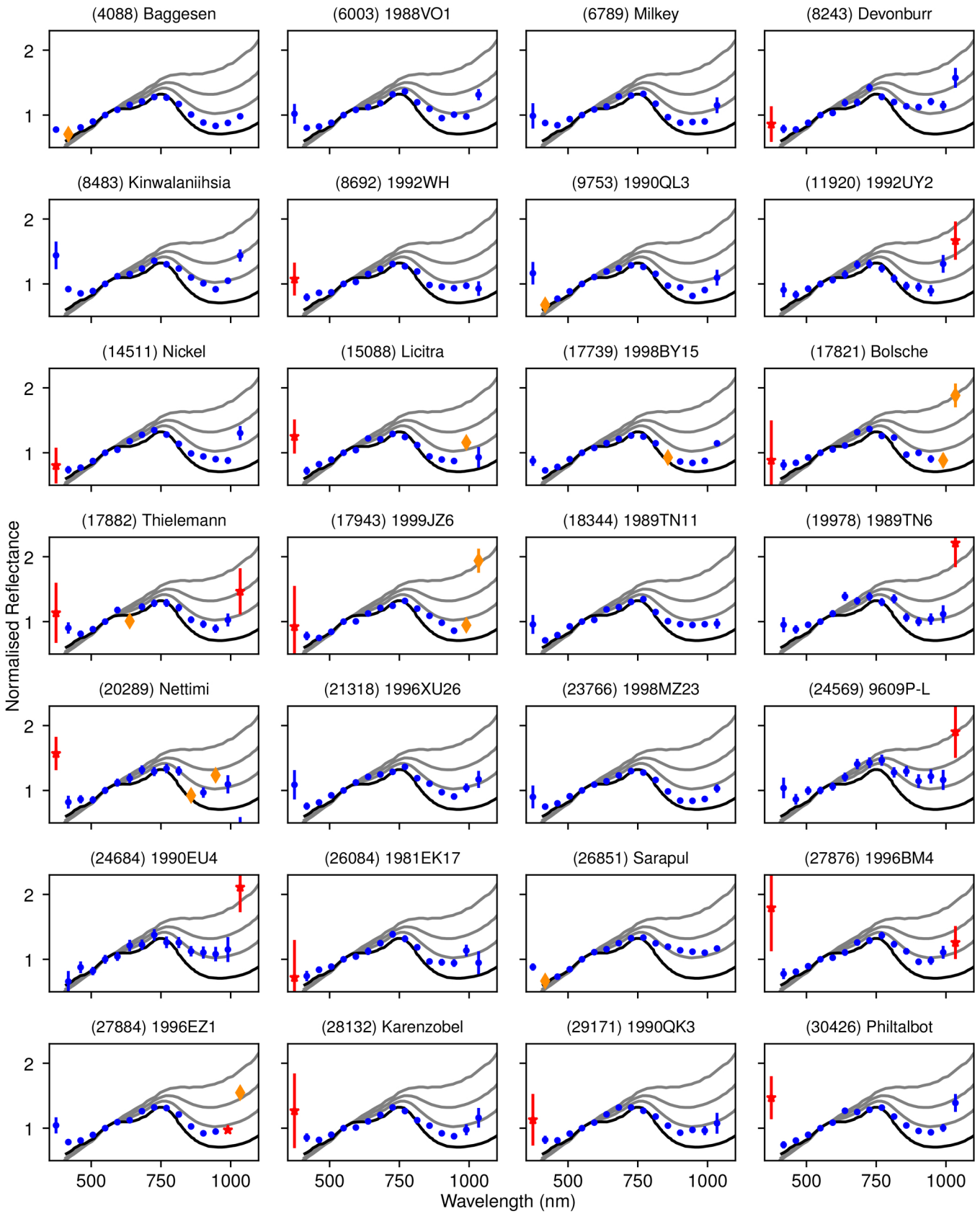

Fig. B.2. Same as Fig. B.1 but with the 56 asteroids visually validated as matches of the low space-weathered EC 002. The space-weathered spectra of EC 002 are shown in grey lines.

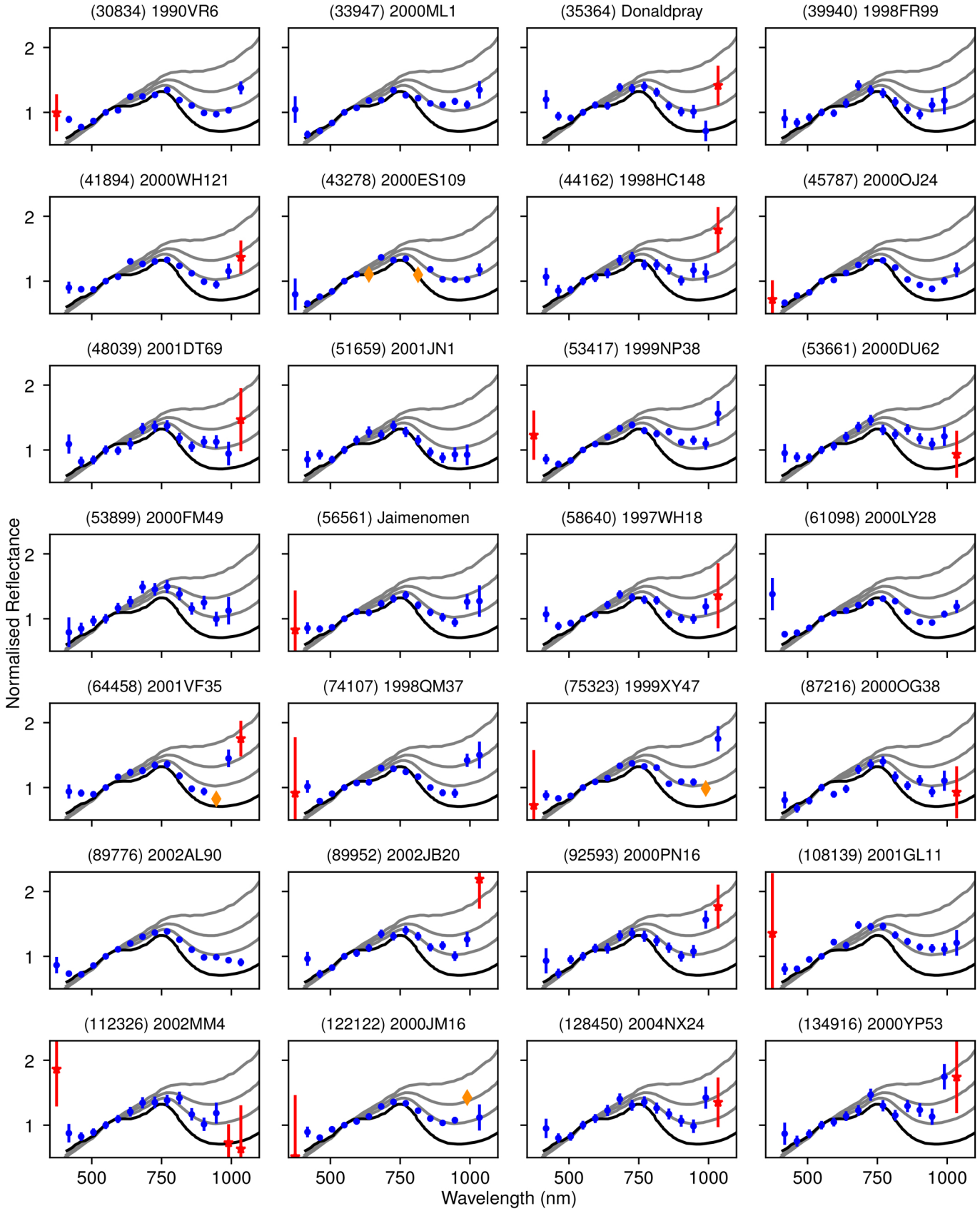

Fig. B.2. continued.

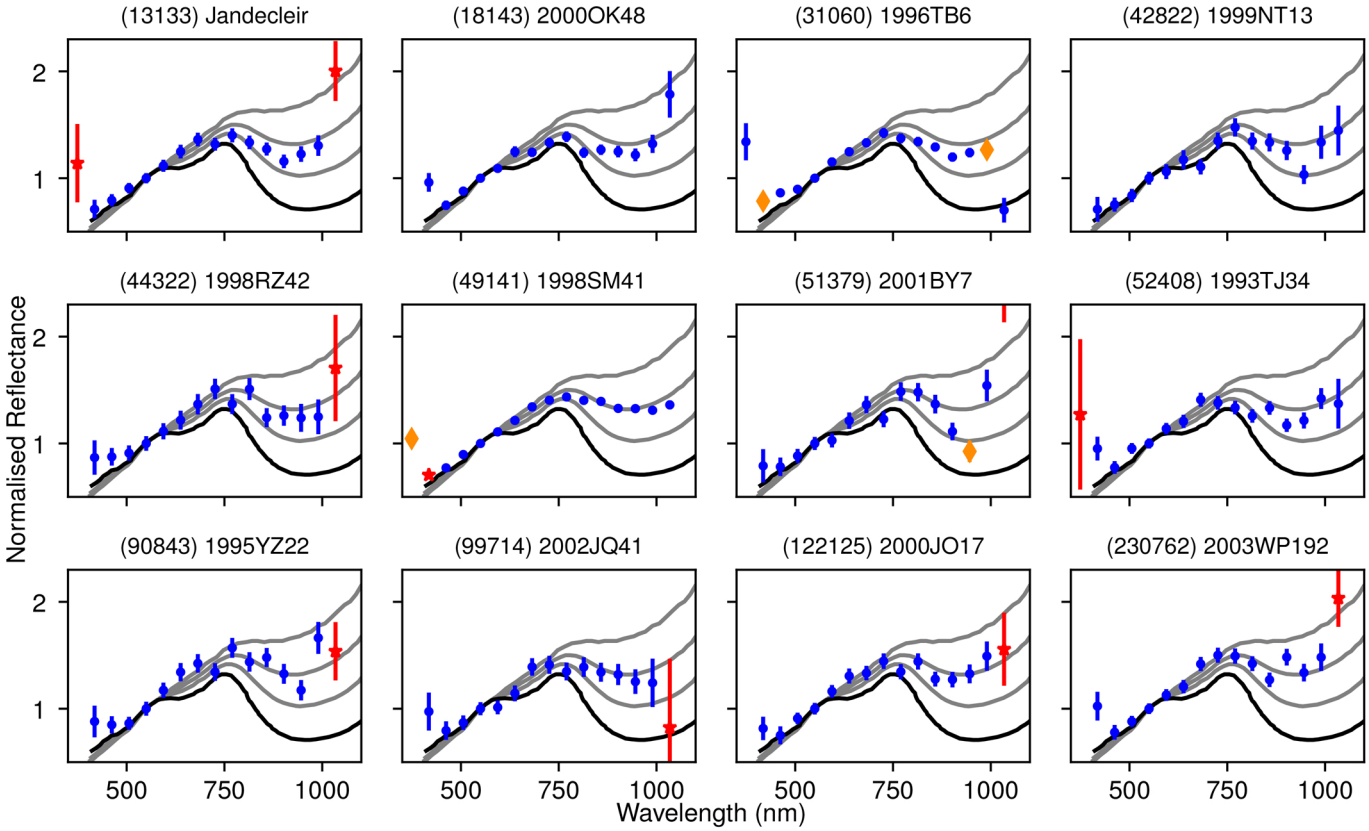

Fig. B.3. Same as Fig. B.2 but with the 12 asteroids visually validated as matches of the medium space-weathered EC 002.

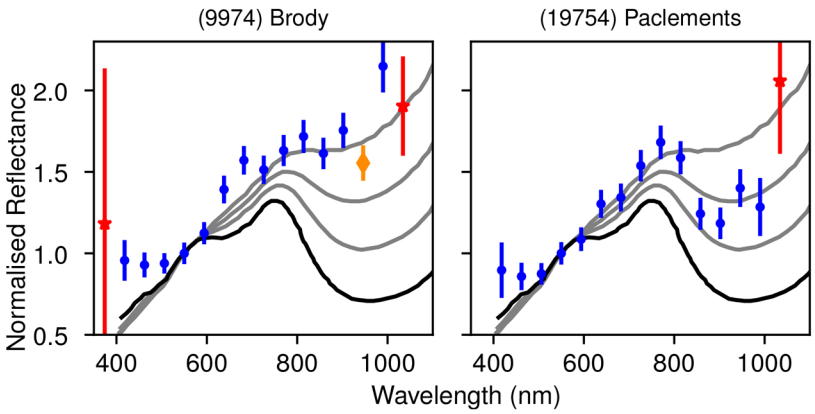

Fig. B.4. Same as Fig. B.2 but with the two asteroids visually validated as matches of the high space-weathered EC 002.

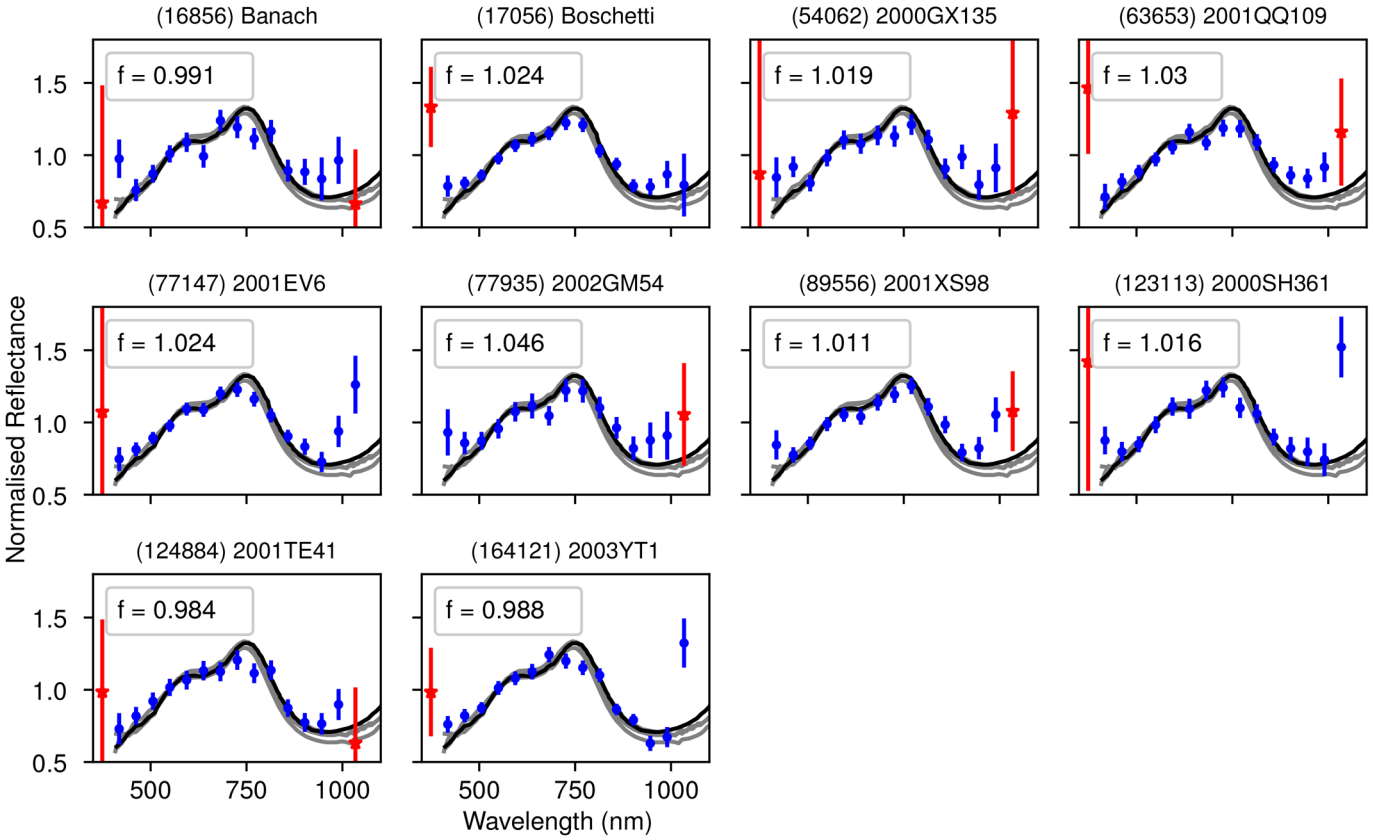

Fig. B.5. Spectra of the ten asteroids found with the curve matching method only, validated as matches of EC 002 after visual inspection. The spectra are normalised with a scaling factor f, here the meteorite spectrum was divided by the scaling factor. The spectra of the powder sample of the meteorite is shown in black continuous line, and the raw slab samples spectra are shown in grey lines. As previously, the 16 bands of the Gaia asteroid spectra are shown with a colour and a symbol associated to their flag number.

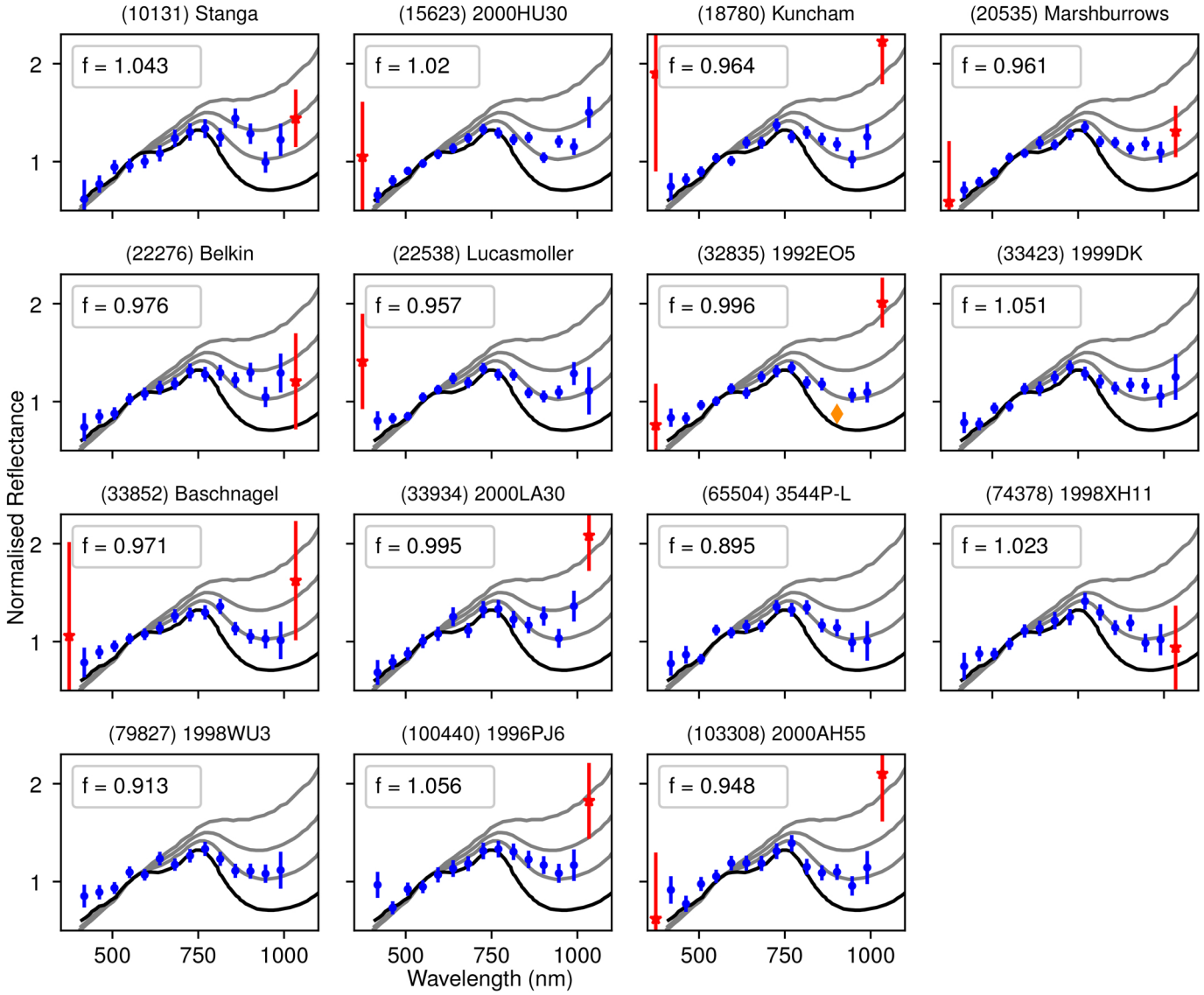

Fig. B.6. Same as Fig. B.5 but with the 15 asteroids visually validated as matches of the low space-weathered EC 002. Here the spectra of the powder sample of the meteorite is shown in black continuous line, and the space-weathered spectra are shown in grey lines.

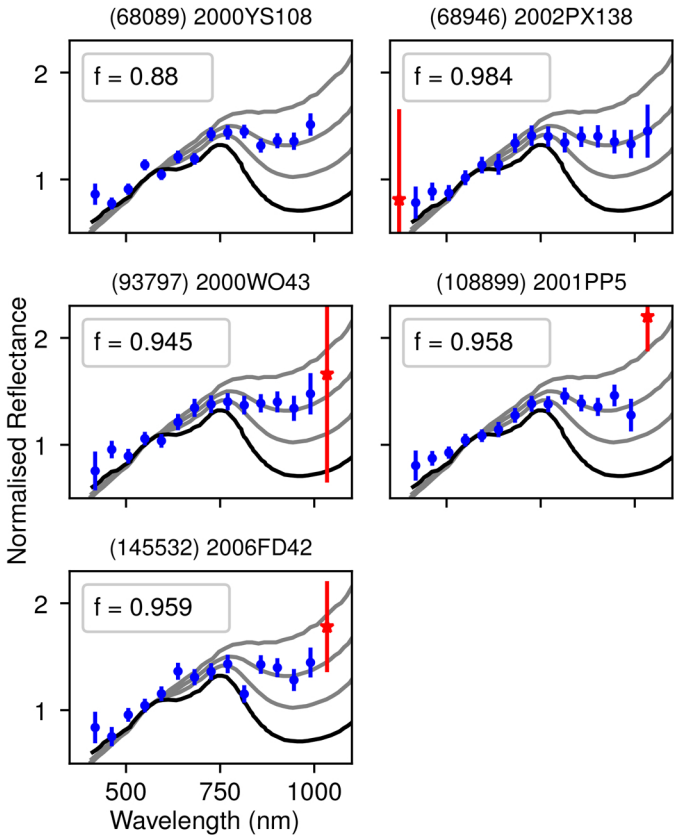

Fig. B.7. Same as Fig. B.6 but with the 8 asteroids visually validated as matches of the medium space-weathered EC 002.

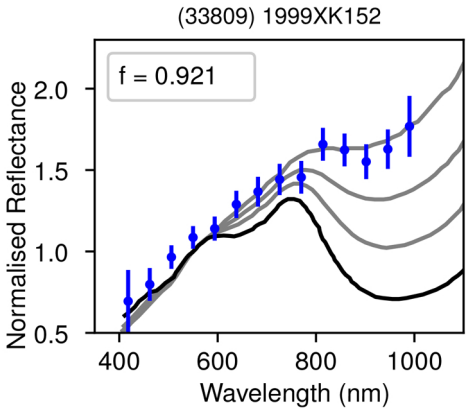

Fig. B.8. Same as Fig. B.6 but with the asteroid visually validated as match of the high space-weathered EC 002.